

# The seismic signature of lithospheric deformation beneath eastern North America due to Grenville and Appalachian orogenesis

Maureen D. Long<sup>1,\*</sup>, Heather A. Ford<sup>1,†</sup>, Lauren Abrahams<sup>1,2</sup>, and Erin A. Wirth<sup>3</sup>

<sup>1</sup>DEPARTMENT OF GEOLOGY AND GEOPHYSICS, YALE UNIVERSITY, PO BOX 208109, NEW HAVEN, CONNECTICUT 06520, USA

<sup>2</sup>DEPARTMENT OF GEOSCIENCE, UNIVERSITY OF WISCONSIN, MADISON, 1215 WEST DAYTON STREET, MADISON, WISCONSIN 53706, USA

<sup>3</sup>DEPARTMENT OF EARTH AND SPACE SCIENCES, UNIVERSITY OF WASHINGTON, 4000 15<sup>TH</sup> AVENUE NE, SEATTLE, WASHINGTON 98195, USA

## ABSTRACT

The eastern margin of North America has been affected by two complete Wilson cycles of supercontinental assembly and breakup over the past ~1.3 b.y. Evidence of these processes is apparent in the surface geology; however, the geometry, strength, and extent of lithospheric deformation associated with these events are poorly known. Observations of seismic anisotropy in the continental lithosphere can shed light on past deformation processes, but information about the depth distribution of anisotropy is needed. Here we investigate the azimuthal dependence of transverse component receiver functions at broadband seismic stations in eastern North America to constrain sharp contrasts in seismic anisotropy with depth. We examined data from six permanent seismic stations, including three that are just to the east of the Grenville Front and three that are within the Appalachian Mountains. A harmonic stacking modeling method was used to constrain the presence of anisotropic interfaces within the crust and mantle lithosphere. A comparison among stations located to the east and to the west of the Grenville Front reveals evidence for different lithospheric anisotropy across the front, which in turn argues for significant lithospheric deformation associated with the Grenville orogeny. Stations located in the Appalachians exhibit a striking signature of strong and multi-layered anisotropy in the lower crust, consistent with observations in modern orogens, as well as the lithospheric mantle. Our observations constrain the existence and approximate depths of contrasts in anisotropy within the lithosphere and may be used for future testing of specific hypotheses regarding lithospheric deformation associated with orogenesis.

LITHOSPHERE

GSA Data Repository Item 2017351

<https://doi.org/10.1130/L660.1>

## INTRODUCTION

The formation of mountain belts at convergent plate boundaries is one of the fundamental processes in plate tectonics. Despite the importance of orogenesis to the plate tectonic system, our understanding of how deformation is accommodated in the crust and mantle lithosphere during orogenesis remains poorly understood. This is true both in present-day orogenic systems and in regions that have been affected by past orogenic events. Lithospheric deformation during orogenesis, while poorly understood, is crucial for our understanding of the evolution of topography, the partitioning of strain in collisional settings, and the evolution and modification of continental margins such as eastern North America. Furthermore, lithospheric deformation reflects

the rheology of the crust and mantle lithosphere, which remain poorly understood despite extensive study.

One type of observation that can inform our view of deformation in the lower crust and upper mantle is seismic anisotropy, or the directional dependence of seismic wave propagation. This is because there is a direct, albeit complicated, link between strain and the resulting seismic anisotropy via the crystallographic preferred orientation (CPO) of anisotropic minerals. In the upper mantle, seismic anisotropy primarily reflects the CPO of olivine (e.g., Karato et al., 2008), while in the lower crust there might be contributions from amphiboles, micas, and/or quartz (e.g., Ward et al., 2012; Liu et al., 2015; Ko and Jung, 2015). There are many published observations of seismic anisotropy within continental settings in general (e.g., Fouch and Ron-denay, 2006; Tommasi and Vauchez, 2015), and beneath eastern North America in particular (e.g., Barruol et al., 1997; Levin et al., 1999; Wagner et al., 2012; Long et al., 2010, 2016; Yang et al.,

2017). A challenge in their interpretation, however, is that it is often difficult to obtain good constraints on the depth extent of anisotropy. For example, the splitting or birefringence of SKS waves (that is, waves that travel as shear waves through the mantle but as compressional waves through the core), perhaps the most common method for studying continental anisotropy, is a path-integrated measurement involving nearly vertically propagating shear waves, so its depth resolution is poor (e.g., Long and Silver, 2009). Complementary constraints on anisotropy can be obtained from surface wave dispersion analysis (e.g., Deschamps et al., 2008; Yuan and Romanowicz, 2010) and by combining different types of seismic data (e.g., Yuan and Levin, 2014; Bodin et al., 2016).

One analysis technique that can yield good resolution of the depth distribution of anisotropy within the lithosphere is anisotropic receiver function analysis, which can reveal sharp contrasts in anisotropic structure with depth (e.g., Levin and Park, 1997, 1998; Bostock, 1998;

\*Corresponding author: [maureen.long@yale.edu](mailto:maureen.long@yale.edu)

†Present address: Department of Earth Sciences, University of California, Riverside, 900 University Ave., Riverside, CA, 92521 USA

Frederiksen and Bostock, 2000; Liu and Park, 2017). This technique has recently been applied to data from continental settings; in particular, there are several recent studies that have applied it to study both crustal anisotropy (e.g., Porter et al., 2011; Schulte-Pelkum and Mahan, 2014a; Liu et al., 2015) and anisotropy within the lithospheric mantle (e.g., Yuan and Levin, 2014; Wirth and Long, 2014; Ford et al., 2016). This analysis strategy, which looks for P to SH wave conversions at a dipping and/or anisotropic interface, can provide unambiguous evidence for anisotropy (usually under the assumption of hexagonal symmetry) and constrains the timing of converted waves (and thus the likely depth of the interfaces). A disadvantage of the technique, however, is that the full anisotropic geometry in each layer across an interface cannot be easily deduced from the observations. Detailed forward modeling can identify plausible anisotropic models (e.g., Wirth and Long, 2012, 2014; McCormack et al., 2013), but forward modeling is generally nonunique and computationally expensive, and the tradeoffs among different model parameters are typically strong (e.g., Porter et al., 2011; Wirth et al., 2017). Simplified modeling using harmonic decomposition or similar techniques (e.g., Shiomi and Park, 2008; Bianchi et al., 2010; Schulte-Pelkum and Mahan, 2014a; Liu et al., 2015; Ford et al., 2016; Olugboji and Park, 2016; Park and Levin, 2016) can identify the presence and primary features of dipping and/or anisotropic interfaces without extensive computation of synthetic seismograms.

In this study we examine data from six long-running broadband seismic stations in the eastern United States (Fig. 1) that overlie lithosphere that has been affected by past mountain-building events, i.e., the Grenville and Appalachian orogenies. The goal of this work is to explore the nature and depth extent of deformation of the crust and mantle lithosphere due to orogenesis using the technique of anisotropic receiver function analysis. We apply a harmonic decomposition modeling approach to our computed receiver functions to identify interfaces within the continental lithosphere with a dipping and/or anisotropic character beneath our selected stations. Three of our stations are just to the east of the Grenville Front, which marks the mapped westward extent of deformation during the Grenville orogeny, and three of our stations are situated within the Appalachians. This particular study is motivated by previous work (Wirth and Long, 2014) that identified evidence for a contrast in anisotropy within the mantle lithosphere at stations in the Granite-Rhyolite Province of eastern North America. The comparison of our new results with these previous results, obtained at stations located to the west

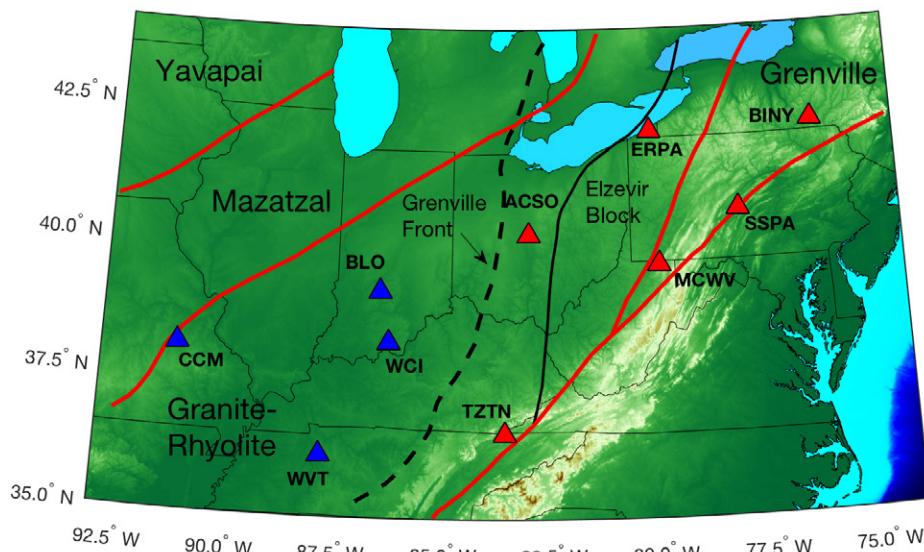


**Figure 1.** Map of station locations and major tectonic boundaries. Red triangles indicate locations of stations used in this study; blue triangles show stations examined by Wirth and Long (2014). Red lines indicate the boundaries of major Proterozoic terranes (Yavapai, Mazatzal, Granite-Rhyolite, and Grenville) according to Whitmeyer and Karlstrom (2007). The dashed line indicates the position of the Grenville deformation front, and the black line indicates the western boundary of the Elzevir block, also from Whitmeyer and Karlstrom (2007).

of the Grenville Front, allows us to investigate whether and how Grenvillian and Appalachian orogenesis modified the anisotropic structure of the lithosphere.

### TECTONIC SETTING OF THE GRENVILLE AND APPALACHIAN OROGENIES

The eastern margin of North America (Fig. 1), today a passive margin in the interior of the North American plate, has been shaped by two complete supercontinent cycles over the past ~1.3 b.y. of Earth history (e.g., Thomas, 2004; Cawood and Buchan, 2007; Benoit et al., 2014). This tectonic history includes multiple and protracted episodes of orogenesis, including the Grenville orogenic cycle that culminated in the formation of the supercontinent Rodinia (e.g., Whitmeyer and Karlstrom, 2007; McLelland et al., 2010) and the Appalachian orogenic cycle that culminated in the formation of the supercontinent Pangea (e.g., Hatcher, 2010; Hibbard et al., 2010). Dispersal of each of these supercontinents was accomplished via continental rifting, including a major diachronous rifting episode between ca. 750 and 550 Ma (e.g., Li et al., 2008; Burton and Southworth, 2010) that broke apart Rodinia and shaped the pre-Appalachian eastern margin of Laurentia (e.g., Allen et al., 2010). The later breakup of Pangea was also accomplished via a complex set of rifting processes that was complete by ca. 190 Ma (e.g., Frizon de Lamotte et al., 2015) but began substantially

earlier (ca. 250 Ma), and was accompanied by voluminous magmatism associated with the Central Atlantic Magmatic Province, a large igneous province (e.g., McHone, 1996, 2000; Schlische et al., 2003). These multiple tectonic episodes were likely accompanied by substantial deformation of the crust and mantle lithosphere as the edges of the (progressively growing) North American continent were modified.

The term Grenville orogeny is used somewhat inconsistently in the literature (e.g., McLelland et al., 2010), but here we use the term to encompass both the Elzevirian orogeny ca. 1.3–1.2 Ga, which sutured the Elzevir block to the Laurentian margin (e.g., Moore and Thompson, 1980; Whitmeyer and Karlstrom, 2007; Bartholomew and Hatcher, 2010), as well as later (ca. 1.09–0.98 Ga; Whitmeyer and Karlstrom, 2007) continent-continent collision that formed Rodinia (e.g., McLelland et al., 1996; Rivers, 1997) as the Grenville Province was joined to Laurentia. The Grenville deformation front, which represents the westward extent of deformation due to Grenvillian orogenesis (e.g., Culotta et al., 1990; Whitmeyer and Karlstrom, 2007), cuts through eastern Michigan and western Ohio and extends to the south and west through Alabama (Fig. 1). In the context of the work presented here, the Grenville Front separates the seismic stations within the Granite-Rhyolite Province examined in Wirth and Long (2014) and those in this study. Of the stations we examine in this study (Fig. 1), station ACSO is located within the

Granite-Rhyolite Province but to the east of the Grenville Front, while station ERPA is located near the suture between the Elzevir block and the rest of the Granite-Rhyolite Province and station BINY is located within the Grenville Province, as defined by Whitmeyer and Karlstrom (2007).

The later Appalachian orogeny, a detailed overview of which was given by Hatcher (2010), involved three distinct phases of orogenesis over a period of several hundred million years, and formed the present-day Appalachian Mountains. The first, the Taconic orogeny, involved the accretion of arc terranes onto the margin of Laurentia between ca. 496 and 428 Ma (Karabinos et al., 1998; Hatcher, 2010), while the later phases (the Acadian-Neocadian and Alleghanian orogenies) involved superterrane accretion (Carolina, Avalon, Gander, and Meguma superterranes, all of peri-Gondwanan affinity) and continental collision. The Acadian orogeny began ca. 410 Ma and primarily affected the northern Appalachians with transpressive north to south collision (e.g., Hatcher, 2010; Ver Straeten, 2010). The Alleghanian orogeny (e.g., Geiser and Engelder, 1983; Sacks and Secor, 1990; Hatcher, 2010; Bartholomew and Whitaker, 2010), which began ca. 300 Ma and was complete by ca. 250 Ma, culminated in the final assembly of the Pangea supercontinent. The protracted series of orogenic events that make up the Appalachian orogenic cycle produced widespread deformation, volcanism, and metamorphism, and produced the topographic signature of the Appalachian Mountains that is still evident today (Hatcher, 2010). Three of the seismic stations that we use in this study (SSPA, MCWV, and TZTN) are located in the Appalachian Mountains, along the edge of the Laurentian core of the North American continent, in regions that were likely affected by deformation associated with Appalachian orogenesis.

## DATA AND METHODS

In this paper we use anisotropic receiver function (RF) analysis to identify and characterize contrasts in seismic anisotropy with depth within the continental crust and mantle lithosphere, following our previous work (Wirth and Long, 2014; Ford et al., 2016). This technique involves the computation of RFs, i.e., a time series that reflects converted seismic phases due to structure beneath a seismic station (e.g., Langston, 1979), for both the radial (oriented in a direction that points from receiver to source) and transverse (oriented orthogonal to the radial) horizontal components of a seismogram. For the case of horizontal interfaces and purely isotropic structure, all of the P to S converted energy would be expected to arrive on the radial

component, as the P and SV wavefields are coupled and (in this case) propagate independently of the SH wavefield. When dipping interfaces or anisotropic structure are present, some of the P to S converted energy will arrive on the transverse component due to P to SH conversions (e.g., Levin and Park, 1997, 1998). For the case of a dipping isotropic interface, these converted waves will manifest as an arrival on the transverse component RF trace that changes polarity twice across the full backazimuthal range (i.e., a two-lobed polarity flip). For the case of a contrast in anisotropy (with a hexagonal symmetry and a horizontal symmetry axis), these conversions will manifest as an arrival on the transverse component RF trace that changes polarity four times across the full backazimuthal range (i.e., a four-lobed polarity flip). For the case of a contrast in anisotropy with a plunging axis of symmetry, a mix of two-lobe and four-lobe polarity changes on the transverse component RFs is predicted. One way to distinguish between a dipping (isotropic) interface and a contrast in anisotropy with a plunging symmetry axis, at least in theory, is to examine the transverse components in the time range associated with the direct P arrival. For a dipping interface, a change in polarity on the transverse components at a time associated with the P to S conversion at an interface will be accompanied by an arrival with the opposite polarity at time  $t = 0$ ; for a contrast in anisotropy at depth, this zero-time arrival is not present. One caveat, however, is that this analysis is complicated when there are multiple interfaces at depth, because multiple zero-time arrivals may interfere. Predicted RF patterns for a suite of simple models that illustrate these ideas were

shown and discussed in detail in Schulte-Pelkum and Mahan (2014b) and Ford et al. (2016).

We selected six long-running broadband seismic stations in the eastern United States for analysis in this study, all part of the permanent U.S. National Seismic Network or Global Seismographic Network (Fig. 1). In order to achieve good azimuthal coverage, we focus on a small number of high-quality stations with long run times. Of these, stations ACSO, ERPA, and BINY are located in regions that were likely affected by Grenville orogenesis, as described here; we collectively refer to these as the Grenville stations in this study. Stations MCWV, SSPA, and TZTN are located in regions of present-day mountainous topography that were likely affected by Appalachian orogenesis (Mountain stations). We examined at least 10 yr of data at each station, selecting events of magnitude 5.8 and greater at epicentral distances between  $30^\circ$  and  $100^\circ$  (Fig. 2) for analysis.

Our preprocessing methodology is identical to that of Ford et al. (2016); each seismogram trace was cut to identical length, rotated into vertical, radial, and transverse components, and bandpass filtered between 0.02 and 2 Hz for P wave picking. We visually inspected each trace for a clear P wave arrival, discarding those traces that did not display an unambiguous P wave, and manually picked the P arrival using the Seismic Analysis Code (SAC) software (<http://ds.iris.edu/ds/nodes/dmc/software/downloads/sac/>). Before computing RFs, we rotated the components into the LQT (theoretical directions of P, SV, and SH motions) reference frame (using a near-surface P wave velocity of 3.5 km/s) to account for the fact that the

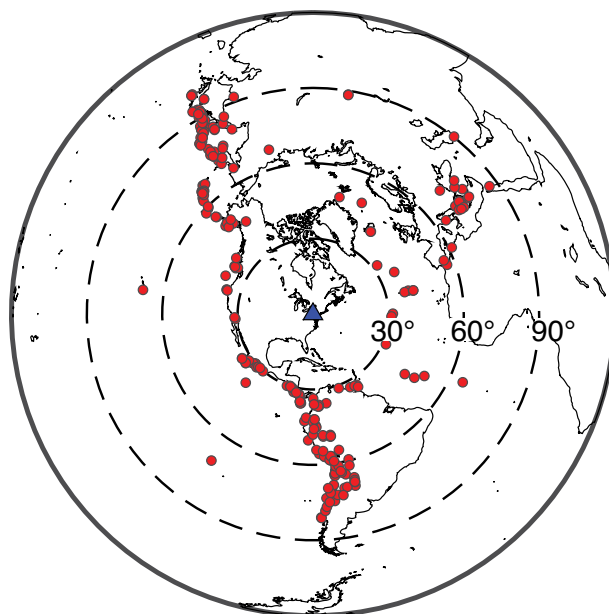


**Figure 2.** Map of earthquakes used in our analysis at station SSPA. Station location is shown with a triangle; event locations are shown with circles. Event distributions for other stations in the study are similar.

incoming P arrivals are not perfectly vertical, again following Ford et al. (2016). We note that while all RFs were computed in the LQT coordinate system, for simplicity we refer to radial and transverse RFs to follow common terminology conventions (e.g., Levin and Park, 1997, 1998). We emphasize, however, that the LQT and RTZ (radial, transverse, vertical) coordinate systems are not strictly equivalent, and that our rotation into the LQT coordinate system is imperfect, because we used a single representative near-surface velocity to calculate the rotations. Finally, before RF computation, we applied a final bandpass filter to each waveform, using a highpass cutoff of 0.02 Hz and a variable lowpass cutoff of 0.5 or 1 Hz.

To compute radial and transverse component RFs, we used the frequency domain multitaper correlation estimator of Park and Levin (2000), which is a commonly applied RF computation technique (recent examples can be found in Wirth and Long, 2012, 2014; McCormack et al., 2013; Yuan and Levin, 2014; Liu et al., 2015; Levin et al., 2016; Olugboji and Park, 2016; Ford et al., 2016). Following Ford et al. (2016), we computed individual RFs and then stacked after corrections for variations in slowness of the direct P wave arrival, which depends on epicentral distance. We computed single-station radial component stacks over all backazimuths, as well as stacks of both radial and transverse component RFs as a function both epicentral

distance (which allows us to evaluate the effects of multiply reflected waves on our results) and backazimuth (which allows us to identify dipping and/or anisotropic structure). Our stacking and plotting conventions are shown in Figure 3, which illustrates a set of RF stacks and plots at station SSPA as an example. In addition to the RF stacks shown in Figures 3A and 3B, we also visualize the backazimuthal variability in transverse component RF energy within specific time ranges (corresponding to specific depth ranges within the lithosphere) using rose diagrams, following the convention in Wirth and Long (2014) and as illustrated in Figure 3D. This plotting convention allows for visual inspection of the azimuthal variability in polarity (represented

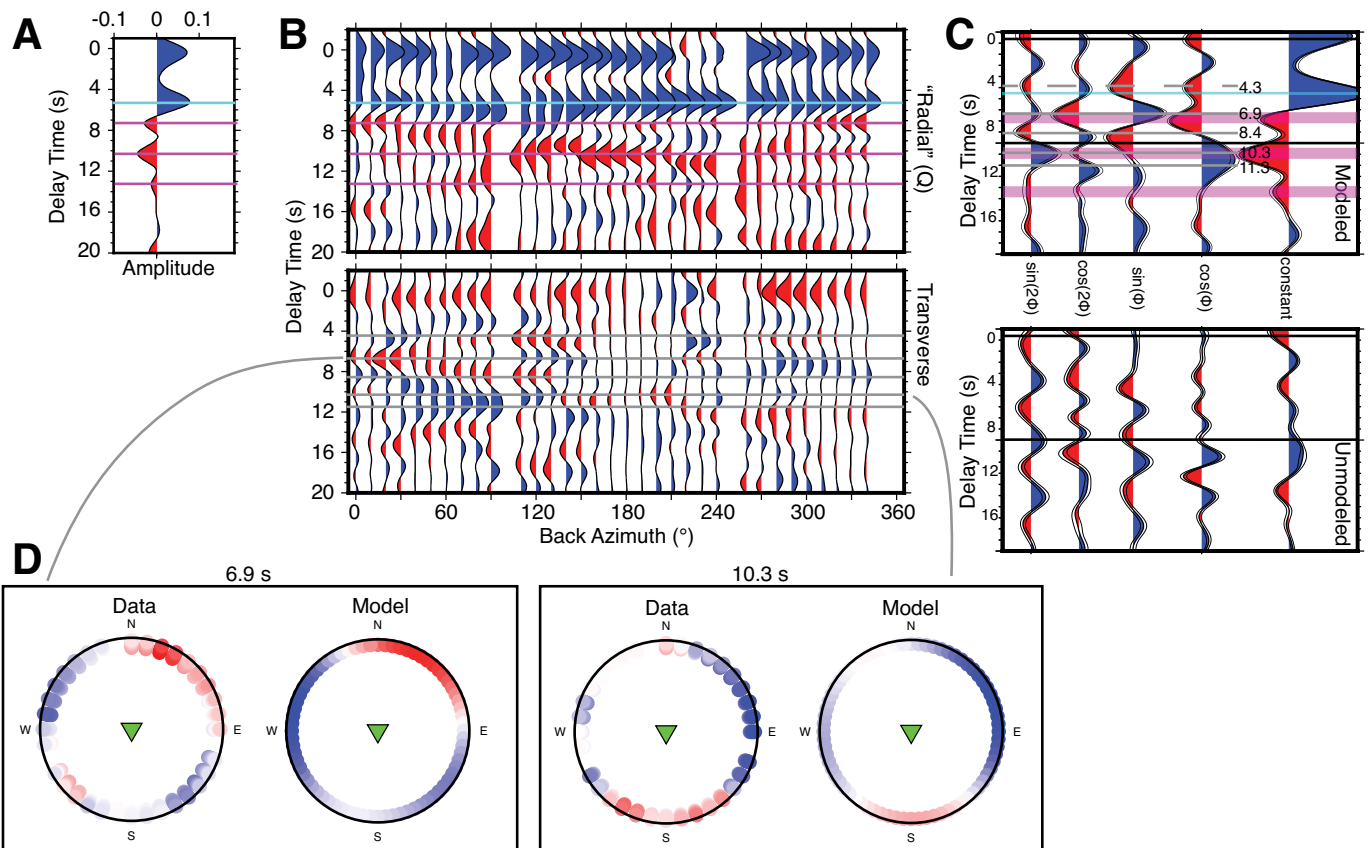


**Figure 3.** Example of different stacking and plotting conventions for station SSPA. (A) Single station stacked, radial component Ps receiver function. The Moho pick is shown with a cyan line, while conversions that may correspond to potential mid-lithospheric discontinuities (MLDs) are shown with magenta lines. (B) Radial (top) and transverse (bottom) component receiver functions binned as a function of back azimuth. Cyan and magenta lines on the top panel correspond to the arrivals picked in panel A. Gray lines on the bottom panel correspond to anisotropic interfaces selected from the regression in C. (C) Harmonic expansion results. Top panel corresponds to the modeled portion of the harmonic expansion, with (from right to left) the  $k = 0$ ,  $k = 1$ , and  $k = 2$  terms shown (as labeled on the bottom of the plot). The bottom panel corresponds to the portion of the Ps receiver function that cannot be modeled by the harmonic expansion. Receiver functions are plotted as a function of delay time relative to the P wave arrival time. A target depth of 90 km was used in the harmonic expansion, and the 90 km and 0 km marks are drawn as horizontal black lines in all panels. Horizontal gray lines in the modeled stacks correspond to interfaces whose presence is inferred from the harmonic stacking results, with numbers showing their arrival times relative to the P wave arrival. Dashed gray lines indicate interfaces at crustal depths; solid gray lines indicate mantle interfaces. Cyan line shows the Moho pick, as in A. Magenta bars show the time range associated with likely MLD arrivals, as in panel A. (D) Example transverse component Ps receiver function rose plots for inferred anisotropic boundaries at 6.9 and 10.3 s. Data are shown on the left of each time increment; the associated model from the harmonic expansion is shown on the right. We note the similarity between our backazimuthal receiver function gathers for station SSPA (panel B) and those presented in Yuan and Levin (2014) (their Fig. 7), who also examined data from this station.

with blue and red colors) at specific time (depth) ranges. The character of any variability (two lobed, four lobed, or a mixture) sheds light on the type of interface (dipping, anisotropic, or both). Distinguishing between a dipping interface and a plunging axis of anisotropy requires an inspection of the transverse component RFs at the arrival time of the direct P wave, as noted here, although in the presence of multiple interfaces this can be difficult.

We implement a harmonic decomposition technique (Shiomi and Park, 2008; Bianchi et al., 2010; Park and Levin, 2016) that allows for the straightforward identification of time ranges within the RF traces that are likely associated with conversions at interfaces of different character. Specifically, harmonic decomposition identifies coherent energy on the RF traces that correspond to arrivals that are constant across backazimuth, that vary as a function of  $\cos(\theta)$  or  $\sin(\theta)$  (where  $\theta$  is backazimuth), that vary as a function of  $\cos(2\theta)$  or  $\sin(2\theta)$ , or a combination of these. Harmonic decomposition modeling thus serves as a useful complement to the simple visual inspection of backazimuthal RF gathers, and has been applied by several recent studies (e.g., Liu et al., 2015; Olugboji and Park, 2016; Ford et al., 2016). A detailed description of our implementation of harmonic decomposition can be found in Ford et al. (2016) and a recent technical overview was given by Park and Levin (2016). Briefly, for each time window the stacked RFs (both radial and transverse components) are modeled as a linear combination of  $\sin(k\theta)$  and  $\cos(k\theta)$  terms (after application of a phase shift that depends on  $k$ ), where  $k = 0, 1$ , or  $2$ . The  $k = 0$  term, with no backazimuthal dependence, suggests an isotropic velocity change across a flat interface; the  $k = 1$  terms imply a dipping interface and/or a dipping axis of anisotropic symmetry; the  $k = 2$  terms correspond to contrast in anisotropy. The harmonic stacking technique is illustrated for example station SSPA in Figure 3, which shows the modeled harmonic decomposition as a function of time (along with an error estimate derived from bootstrap resampling; see Ford et al., 2016 for details). Figure 3 also shows the unmodeled portion of the signal, which cannot be represented as a linear sum of  $\sin(k\theta)$  and  $\cos(k\theta)$  terms. Here the unmodeled components for each value of  $k$  represent the portion of the signal that has the opposite phase shift as that of the harmonic expansion model (Shiomi and Park, 2008).

## RESULTS

For each of the six stations examined in this study, we computed stacked radial RFs over all backazimuths for two different lowpass

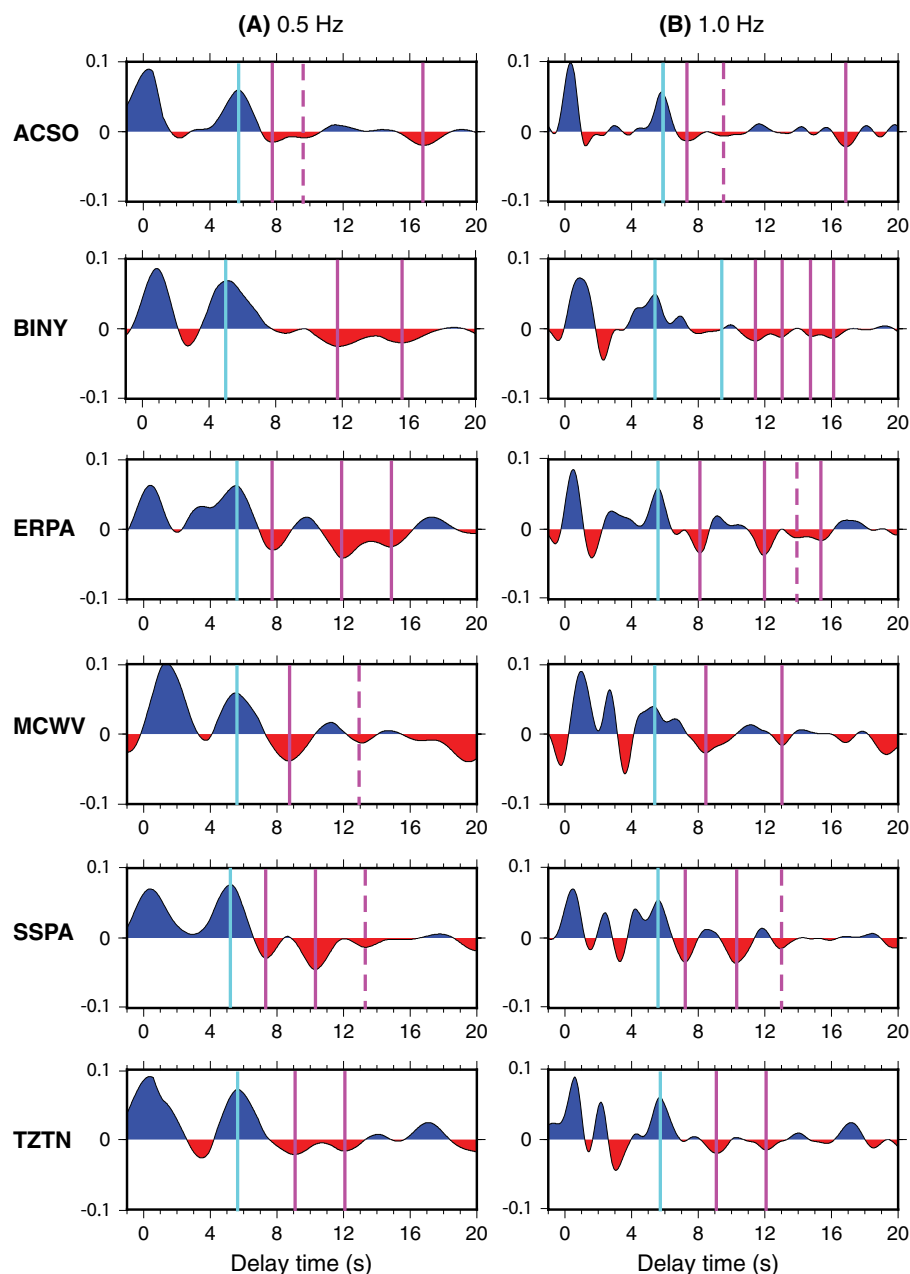


**Figure 4.** Station-stacked, radial component  $P_s$  receiver functions shown for all stations. (A) Filtered at 0.5 Hz. (B) Filtered at 1.0 Hz. Y-axis for each panel is delay time (relative to direct  $P$  arrival) in seconds. Blue phases indicate positive amplitudes and an inferred velocity increase with depth; red indicates negative amplitudes and an inferred velocity decrease with depth. Station names are shown on the far left. The Moho picks are shown in cyan and the negative picks interpreted as either mid-lithospheric discontinuities or lithosphere-asthenosphere boundary are shown in magenta; dashed lines indicate interfaces with smaller amplitudes.

frequency cutoffs (Fig. 4) as well as backazimuthal and epicentral distance gathers (GSA Data Repository Figs. S1–S12<sup>1</sup>). Here we focus our presentation of the results and discussion of

our interpretation on the single-station stacked radial RFs (Fig. 4) as well as the harmonic decomposition results for each station, grouped by region (Grenville stations in Fig. 5 and Mountain stations in Fig. 6). We use the harmonic decomposition modeling to guide our interpretation of major interfaces and their anisotropic or isotropic character beneath each station, as shown in Figs. 7 and 8 and discussed in the

<sup>1</sup>GSA Data Repository Item 2017351, containing Supplemental Figures S1–S12 and captions, is available at <http://www.geosociety.org/datarepository/2017>, or on request from [editing@geosociety.org](mailto:editing@geosociety.org).

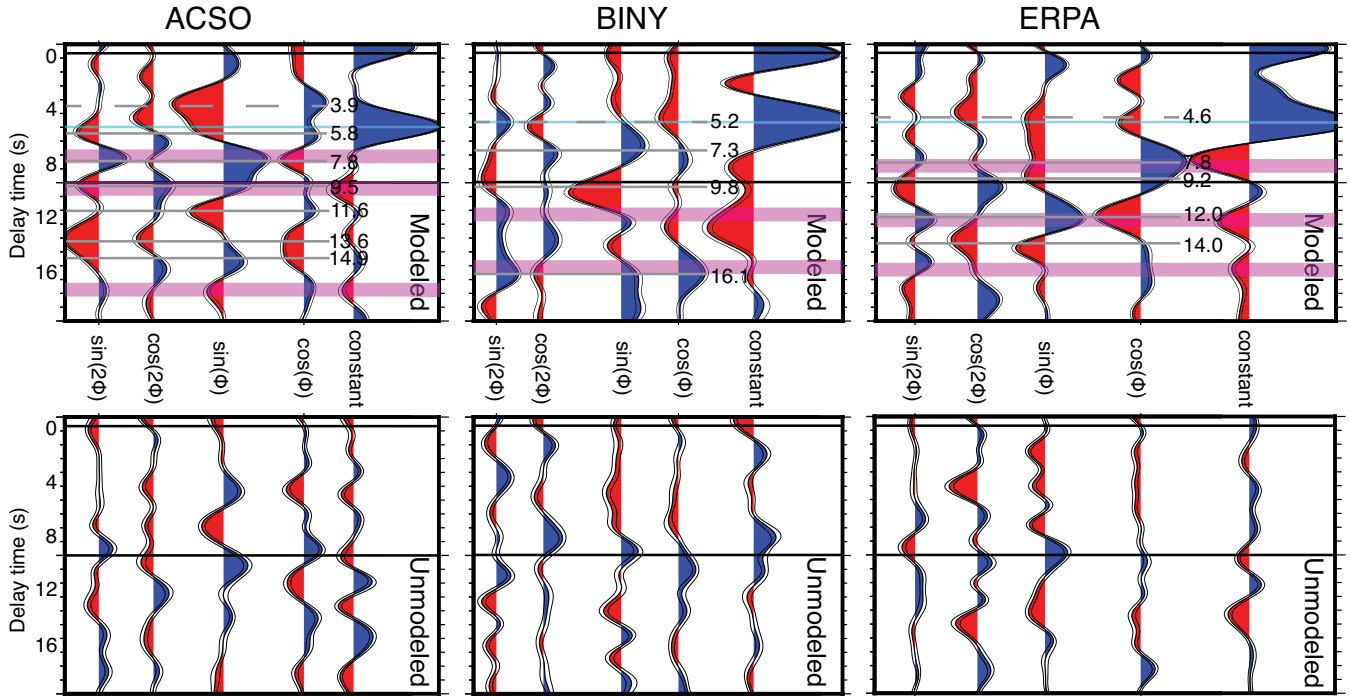


Figure 5. Ps receiver functions binned as a function of harmonic expansion terms for Grenville Province stations ACSO, BINY, and ERPA. Top panels correspond to the modeled portion of the harmonic expansion. The bottom panels correspond to the portion of the Ps receiver functions that cannot be modeled via harmonic expansion. Both the modeled and unmodeled receiver functions (RF) are plotted as a function of delay time relative to the direct P wave arrival. A target migration depth of 90 km was used in the harmonic expansion (e.g., Bianchi et al., 2010; Ford et al., 2016), and the 90 km and 0 km marks are drawn as horizontal black lines in all panels. Gray solid lines mark the location of significant anisotropic boundaries within the mantle and are labeled with the delay time relative to the direct P arrival. Gray dashed lines mark the location of anisotropic boundaries at or above the Moho. Rose plots that display the transverse component RF energy as a function of backazimuth for the time window associated with these boundaries are shown in Figures 7 and 8. Magenta bars correspond to approximate mid-lithospheric discontinuity and/or lithosphere-asthenosphere boundary arrival delay times ( $\pm 0.5$  s). The cyan line corresponds to the Moho arrival.

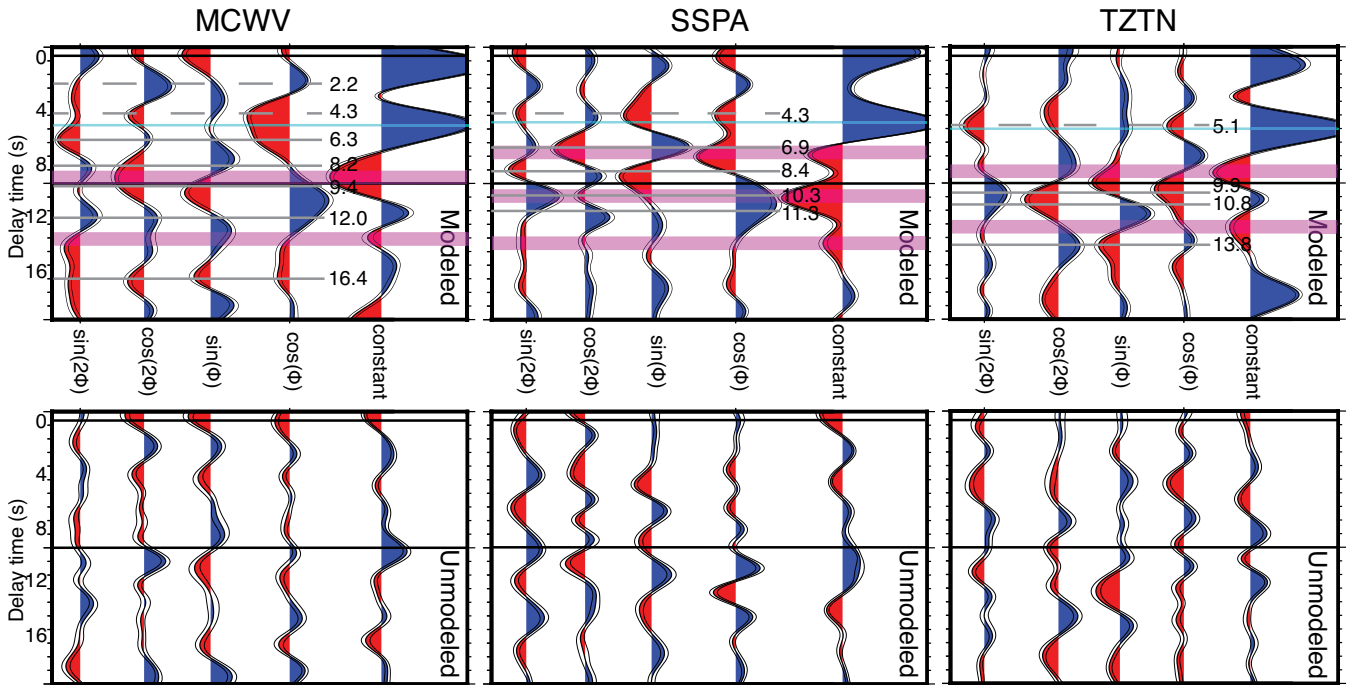
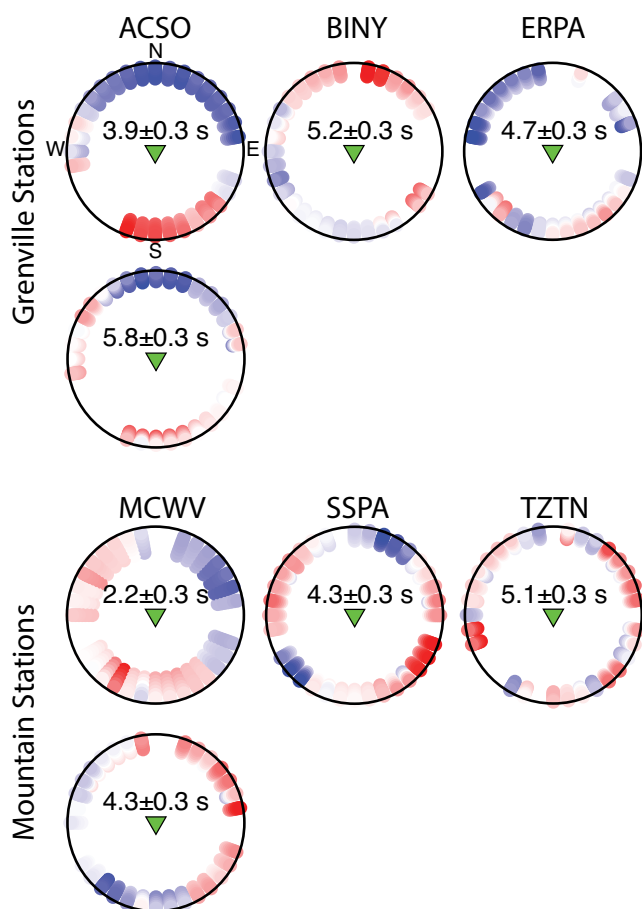


Figure 6. Ps receiver functions binned as a function of harmonic expansion terms for Appalachian stations MCWV, SSPA, and TZTN. Plotting conventions are as in Figure 5. Rose plots that display the transverse component receiver function energy as a function of backazimuth for the time window associated with the boundaries marked in gray are shown in Figures 7 and 8.



**Figure 7. Transverse component Ps receiver function rose plots for inferred anisotropic boundaries within the crust, as inferred from the harmonic expansion shown in Figures 5 and 6. Stations are grouped according to location (Grenville or Mountain stations). Each individual rose plot shows the transverse component amplitudes as a function of backazimuth at the given delay time. Individual rose plots were normalized such that the maximum amplitude within each plot is equal to one.**

following. While we do not discuss the epicentral distance gathers in detail, for each of the interfaces that we interpret in this paper, we have checked the epicentral distance gathers (odd numbered Figs. S1–S12) to ensure that these arrivals do not exhibit moveout that suggests that they are contaminated by multiply reflected waves from the crust. We note that while our use of the LQT coordinate system should theoretically remove the direct P arrival from our RF stacks, some energy at or near  $t = 0$  is often visible (Fig. 4; Figs. S1–S12). This reflects minor inaccuracies in the velocity model used to predict the geometry of the incident P wave; an offset from  $t = 0$  in this arrival (e.g., stations BINY and MCWV in Fig. 4) may reflect the presence of thick sedimentary cover beneath the stations or (more likely) shallow intracrustal interfaces.

The stacked radial RFs shown in Figure 4, which reflect events arriving across the full backazimuthal range and thus obscure any dipping or anisotropic structure, yield evidence for complex structure with a number of interfaces beneath each of the stations examined in this study. At our lower frequency range (lowpass cutoff at 0.5 Hz; Fig. 4A), we observe at all stations a strong, clear positive pulse (light blue lines in Fig. 4)

~5–5.8 s after the P arrival, which we interpret as corresponding to the positive (isotropic) velocity change across the Moho. This time interval corresponds to a crustal thickness of ~38–48 km for reasonable velocity models for continental crust, and is generally consistent with previously published estimates of crustal thickness in our study region (e.g., Abt et al., 2010). In addition to the Moho, we also see evidence for (typically two or more) negative pulses (corresponding to a decrease in velocity with depth) at later time ranges (~8 s and greater; pink lines in Fig. 4), which may correspond either to mid-lithospheric discontinuities (MLDs; Abt et al., 2010; Ford et al., 2016) or, perhaps, to the base of the lithosphere. When higher frequency energy (as high as 1 Hz) is included, the radial RF stacks (Fig. 4B) have similar character but more detail, often hinting at intracrustal layering (pulses arriving before the Moho conversion).

Figures 5 and 6 show the results of the harmonic decomposition analysis for all stations, computed for our low-frequency data (cutoff frequency of 0.5 Hz, the same as the RFs shown in Figs. S1–S12). Focusing first on the Grenville stations (ACSO, BINY, and ERPA; Fig. 5), we find that the harmonic stacking approach is

generally able to model most of the features of the RFs (note relatively small amplitudes on the unmodeled stacks) and yields evidence for a number of interfaces with different character. Beneath station ACSO, the Moho is expressed as a large-amplitude positive pulse on the constant term (at  $t = 5.8$  s relative to direct P); in the same time window, there is some energy (above the error estimate, shown on each trace) on the  $k = 1$  and  $k = 2$  terms, although it is weaker. Still, the presence of energy on the  $k = 1$  and  $k = 2$  terms arriving at the same time as the constant Moho arrival suggests a contrast in anisotropy across the Moho, perhaps with a dipping symmetry axis, and/or a dipping Moho interface. We also see evidence on the constant term stack for an isotropic velocity drop at a depth internal to the mantle lithosphere ( $t = 9.5$  s, corresponding to ~90 km based on the ak135 Earth model of Kennett et al., 1995); the  $k = 1$  and  $k = 2$  terms in this time range suggest a contrast in anisotropy and/or a dip to this interface as well. This inferred MLD phase does not show a clear moveout in the epicentral distance stacks (Fig. S2), which argues against significant contamination from crustal multiples; a similar argument can be made for each of the mantle interfaces we discuss herein, with one exception noted, as follows.

Returning to the harmonic decomposition analysis in Figure 5 and focusing purely on the  $k = 1$  and  $k = 2$  components, we can identify peaks corresponding to interfaces at mantle depths beneath ACSO that suggest a contrast in anisotropy (perhaps with a dipping symmetry axis), but do not necessarily correspond to high amplitudes on the constant term (meaning an isotropic velocity change is not required). In the time range associated with the direct P arrival, the transverse component RFs show little or no energy at most backazimuths (Fig. S1); we do not observe any convincing zero-time arrivals that might result from a dipping interface, so contrasts in anisotropy with a plunging symmetry axis may be more likely. We emphasize, however, that the presence of multiple interfaces with large  $k = 1$  terms in the harmonic expansion implies that an examination of the zero-time transverse component arrivals to distinguish between dipping interfaces and plunging anisotropy is not straightforward.

Beneath station BINY (Fig. 5), the general character of the inferred interfaces is similar to what we infer beneath ACSO, but the details are different. In the time window corresponding to the Moho pulse ( $t = 5.2$  s) on the constant term, there is clear energy on both the  $\sin(2\theta)$  and  $\cos(2\theta)$  terms, again suggesting a contrast in anisotropy across the Moho. At later times, corresponding to depths internal to the mantle

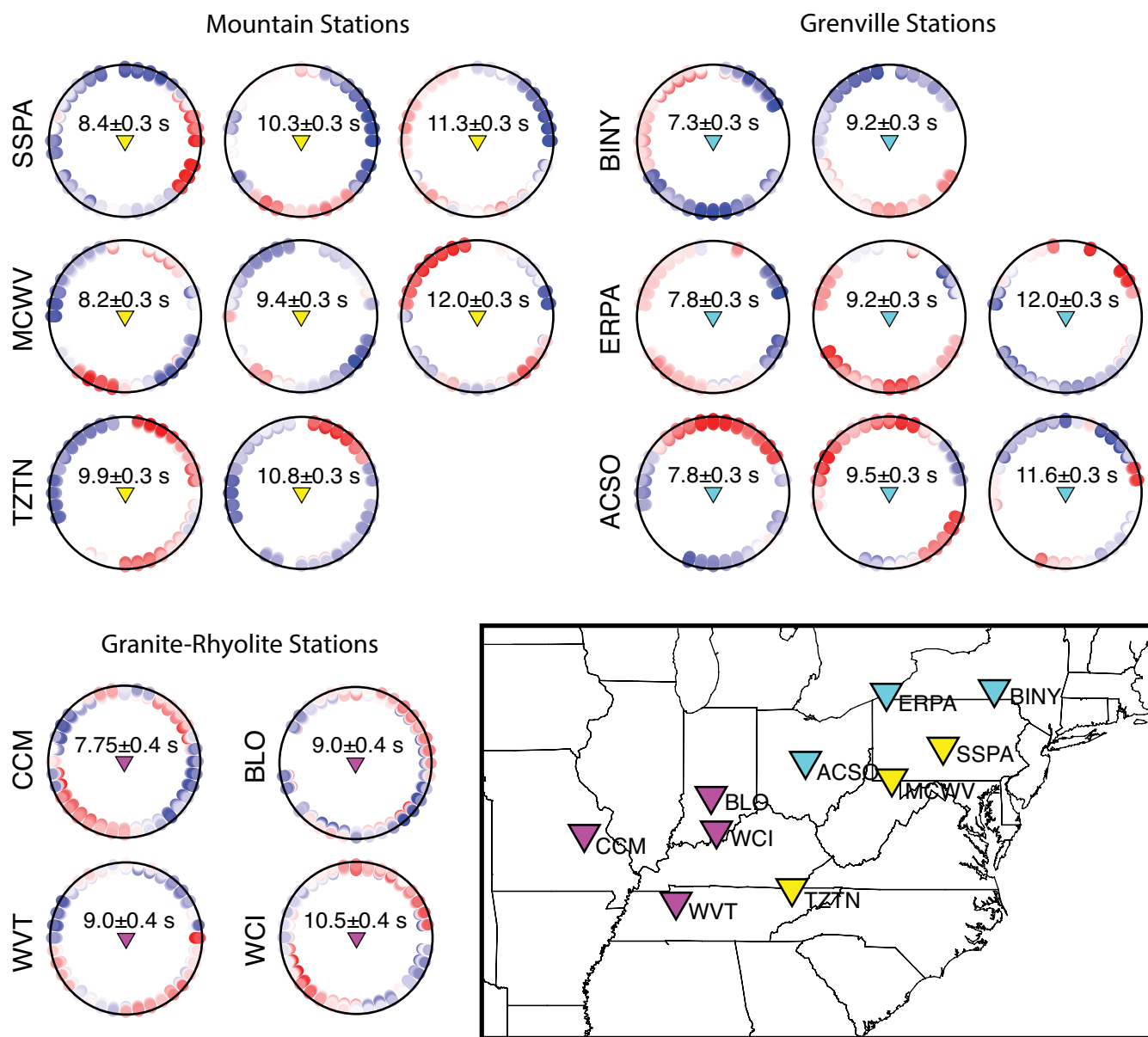


**Figure 8.** Transverse component  $P_s$  receiver function rose plots for inferred anisotropic boundaries within the mantle arriving at  $\sim 7$  s time delay and later, as inferred from the harmonic expansion shown in Figures 5 and 6. The plotting convention is the same as in Figure 7. Rose plots are grouped according to location (Grenville, Granite-Rhyolite, and Mountain stations), and include results for stations within the Granite-Rhyolite Province from our previous work (Wirth and Long, 2014).

lithosphere, we see a number of interfaces evident on both the constant and the higher order ( $k = 1, 2$ ) terms, but the exact timing of these arrivals, and the anisotropic and/or dipping geometry suggested by relative strength of the  $\cos(\theta)$ ,  $\sin(\theta)$ ,  $\cos(2\theta)$ , and  $\sin(2\theta)$  stacks, are different than for station ACSO. Similarly, beneath ERPA, we see the same general pattern, with both isotropic and anisotropic/dipping interfaces suggested by the harmonic decomposition, but with different specific characteristics. It is striking that ERPA exhibits an interface at a time of  $\sim 7.8$

s (relative to direct P;  $\sim 75$ – $80$  km depth based on ak135) that shows both a strong (negative) constant component and a strong  $\cos(\theta)$  component. This strong  $k = 1$  term may correspond to either a dipping MLD or a contrast in anisotropy across the MLD that involves a plunging axis of anisotropy; the very weak signal at zero delay time (relative to P) on the transverse component RFs for this station (Fig. S5) suggests that the latter possibility is more likely. There is another strong negative arrival on the constant stack ( $t = 12$  s;  $\sim 120$  km depth) that also shows large

amplitudes for  $\cos(\theta)$ ,  $\sin(\theta)$ , and  $\sin(2\theta)$ , again suggesting a contrast in anisotropy with a plunging symmetry axis.

Our harmonic stacking results for the Mountain stations (Fig. 6) reveal a series of complicated interfaces, many with dipping and/or anisotropic character, beneath each station. At each of the three stations, we observe a clear Moho arrival on the constant term, and at two of the three stations (SSPA and TZTN), the higher order stacks also exhibit clear peaks in the same time window, suggesting an anisotropic and/or



dipping character to this interface. (At MCWV, there is an anisotropic intracrustal interface whose conversions arrive  $\sim 1$  s ahead of the Moho Ps phase, but it appears to be distinct from the Moho.) The constant terms at each of the three stations at time windows corresponding to mantle depths suggest one or more interfaces with a velocity drop, implying the likely presence of multiple MLDs; typically, these are also associated with an anisotropic or dipping character, as revealed by the higher order terms. For the most part, the epicentral distance gathers argue against contamination of crustal multiples in our interpretation of mantle interfaces beneath these stations, although we observe some moveout for the negative arrival at times near  $t = 9$  s for station TZTN (Fig. S12); its interpretation should therefore be treated with some caution. An examination of the transverse RFs gathers at  $t = 0$  for the Mountain stations (Figs. S7, S9, and S11) reveals modest amounts of energy, with complex backazimuthal patterns. For each of the three stations, there is nonzero energy at  $t = 0$ , suggesting the presence of dipping interfaces at depth, but the azimuthal variability is not clear enough to identify individual two-lobed polarity changes and associate them with specific interfaces.

As with the Grenville stations, we are also able to pick out features on the  $k = 1$  and  $k = 2$  stacks at individual Mountain stations that do not obviously correspond to features on the constant stacks, suggesting that there is some anisotropic layering with the lithosphere that is not accompanied by an isotropic change in velocity. As with the Grenville stations, the collection of harmonic stacks for the Mountain stations, taken as a whole, suggests pronounced differences in the details of both isotropic and anisotropic layering among different stations. Visual inspection of the three stations shown in Figure 6 reveals major differences in the timing and character (i.e., the geometry of polarity reversals as revealed by the harmonic stacking technique) of individual interfaces among different stations.

## INTERPRETATION AND DISCUSSION

A key advantage of the harmonic stacking technique is that it allows us to identify conversions associated with interfaces that exhibit a dipping and/or anisotropic character, a task that is somewhat difficult relying only on visual inspection. From the harmonic stacks shown in Figures 5 and 6, we have picked a series of time ranges (indicated by gray lines in Figs. 5 and 6, with dashed lines for interfaces within the crust and solid lines for interfaces within the mantle) that indicate dipping and/or anisotropic

interfaces beneath each station. Our methodology for picking these interfaces follows Ford et al. (2016) and involves a summation of each of the four nonconstant terms at each delay time in order to determine where coherent peaks in energy occur. Another way of visualizing the character of these interfaces, which lends itself well to comparison among different stations, is to plot rose diagrams (as illustrated in Fig. 3) for each of these time ranges, showing the variability in the transverse component RF polarities and amplitudes as a function of backazimuth. In Figure 7, we show rose diagrams interfaces at crustal depths for each station (either within the crust or collocated with the isotropic Moho), grouped by tectonic setting (Grenville versus Mountain stations). In Figure 8, we show similar rose diagrams for interfaces within the mantle lithosphere; this figure also includes a comparison with data from our previous study using stations within the Granite-Rhyolite Province (Wirth and Long, 2014). We have also used the harmonic decomposition results to calculate azimuthal phase information for individual interfaces (for both the  $k = 1$  and  $k = 2$  terms) that corresponds to the azimuthal location of polarity changes in the rose plots in Figure 7 and 8 and that contains information about the possible dip or plunge directions for a dipping interface or plunging symmetry axis (for the  $k = 1$  components), and information about contrasts in the orientation of horizontal azimuthal anisotropy (for the  $k = 2$  components). These orientations are shown in map view in Figures 9–11, and discussed in detail in the following.

Taken together, the collection of rose diagrams shown in Figures 7 and 8 illustrates that our stations overlie highly complex lithosphere, with a number of interfaces both within the crust and within the mantle lithosphere that dip and/or feature a contrast in anisotropy, perhaps with dipping symmetry axes. This is true both at crustal depths (Fig. 7) and within the mantle lithosphere (Fig. 8), and is similar to our previous findings within Archean cratonic regions of North America (the Wyoming and Superior cratons; Ford et al., 2016). In Ford et al. (2016), we identified a surprising amount of both vertical and lateral heterogeneity in lithospheric structure, suggesting that the complex tectonic processes that produce very heterogeneous structure in the surface geology also produce similarly complex structure within the deep lithosphere. It is strikingly evident from Figures 7 and 8 that there is significant lateral heterogeneity within the crust and lithosphere in our eastern United States study region, even when we compare within groups of stations. Stations that overlie lithosphere likely affected by Grenville orogenesis show little similarity in the timing,

character, or geometry of dipping/anisotropic structure across stations; the same is true for the Mountain stations that overlie lithosphere likely affected by Appalachian orogenesis.

A more detailed examination of the crustal interfaces illustrated in Figure 7 yields some clues as to their geometry and possible origin. Beneath ACSO, we identify a dipping interface within the crust, with conversions arriving  $\sim 3.9$  s after the direct P arrival. The energy on the transverse component RFs at  $t = 0$  may result from this dipping interface, although the azimuthal variability in its polarity is less clear-cut than the azimuthal variability in the Ps arrival at  $\sim 3.9$  s. Lacking a detailed crustal velocity model, we cannot accurately estimate the depth of this interface, but its timing suggests mid-crustal depths. The arrival is modeled well with the  $k = 1$  terms in the harmonic expansion (Fig. 5), so anisotropy need not be invoked. Also beneath ACSO, we see evidence for an anisotropic contrast across the Moho; in the time range ( $\sim 5.8$  s) associated with the constant (isotropic) Moho arrival, the transverse component exhibits significant azimuthal variability (Fig. 7), with a nonzero  $\sin(2\theta)$  term. Visually, the transverse components associated with the Moho arrival look similar to those for the mid-crustal arrival (upper left panels in Fig. 7), but an additional anisotropic component is suggested by the harmonic stacks. Beneath both BINY and ERPA, and similar to ACSO, there is variability on the transverse component in the time range associated with Moho conversions (Fig. 7) that suggests the presence of a contrast in anisotropy (see nonzero  $k = 2$  terms in this time range in the harmonic stacks in Fig. 5) as well as a dipping component. We see evidence for a contrast in anisotropic properties between the lower crust and the uppermost mantle at all three Grenville stations, suggesting anisotropy in one or both layers.

Our inferences on crustal structure beneath the Mountain stations (Fig. 7) include our identification beneath station MCWV of two intracrustal interfaces (at  $\sim 2.2$  s and  $\sim 4.3$  s; both times are before the Moho arrival), each of which exhibit significant energy in both the  $k = 1$  and  $k = 2$  stacks (Fig. 6) and thus require some contribution from anisotropic structure. This observation strongly suggests at the presence of multiple anisotropic layers within the middle to lower crust beneath MCWV, likely with dipping anisotropic symmetry axes (and/or with a dip to the interfaces). Similarly, beneath SSPA, we infer the presence of an interface in the lowermost crust (arrival time  $\sim 4.3$  s, just before the Moho arrival but with  $k = 1$  and  $k = 2$  peaks that clearly arrive before the  $k = 0$  Moho peak; Fig. 6) that also requires a contrast

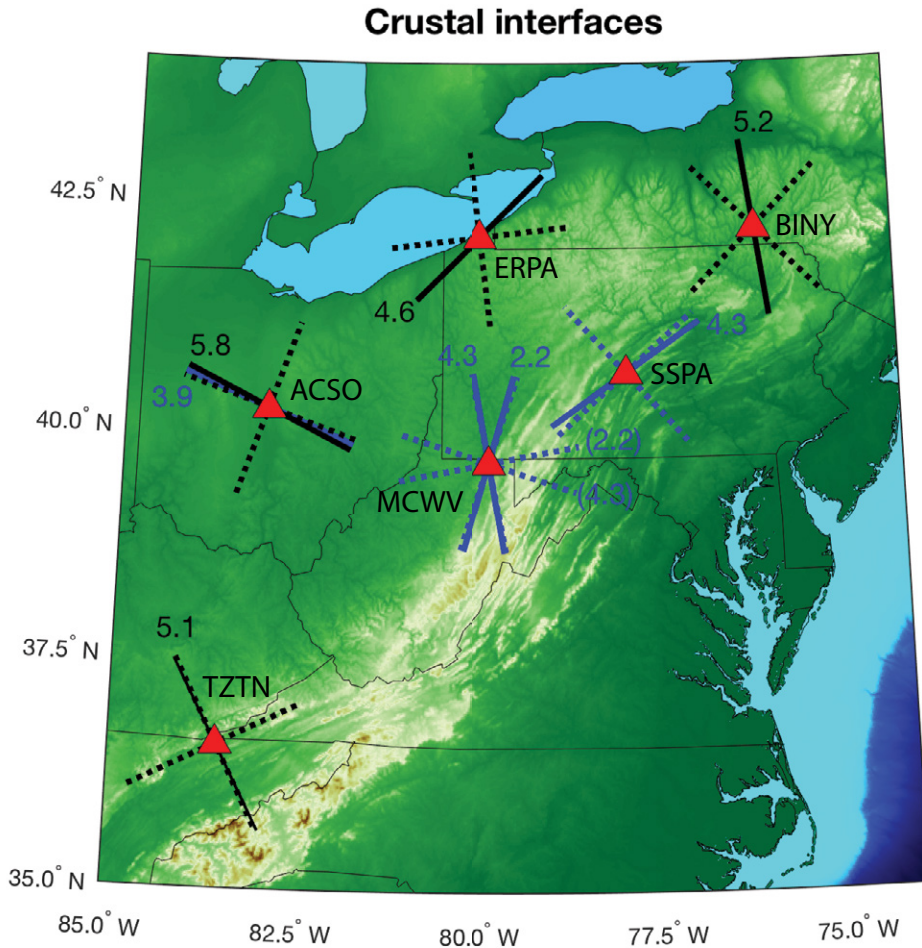


**Figure 9.** Summary map of the properties of crustal interfaces, as derived from the harmonic expansions shown in Figures 5 and 6. Solid lines show the azimuthal phase information (i.e., the azimuthal location of polarity changes in the transverse component receiver functions, RFs) for the  $k = 1$  terms in the harmonic expansion that correspond to possible dip directions (for a dipping interface) or plunge directions (for a dipping anisotropic symmetry axis). Dotted lines show the azimuthal phase information for the  $k = 2$  terms in the harmonic expansion (for interfaces with a strong  $k = 2$  component), which are related to changes in symmetry axis orientations for contrasts in azimuthal anisotropy. Note the  $90^\circ$  ambiguity in the phase orientations for the  $k = 2$  terms, reflecting the four-lobed polarity flip with backazimuth on the transverse component RFs. Blue lines indicate intracrustal interfaces, and black lines correspond to dipping and/or anisotropic contrasts across the Moho. Each of the  $k = 1$  orientations is marked with the arrival time of the Ps converted phase (relative to direct P wave arrival). Note that beneath station MCWV, evidence for a dipping and/or anisotropic component to the Moho interface is ambiguous; however, this station overlies two clear intracrustal interfaces with different geometries, as shown in Figure 7. Similarly, we infer the presence of an anisotropic interface within the deep crust beneath station SSPA. For station MCWV, we have also labeled arrival times for  $k = 2$  components (in parentheses) to distinguish the multiple interfaces. Station ACISO exhibits an intracrustal interface that is well described with only a  $k = 1$  component.

in anisotropy. The rose diagram for this interface (Fig. 7) clearly shows four polarity changes across the full backazimuthal range, although this pattern is modulated by  $k = 1$  terms as well (Fig. 6). Beneath TZTN, the only identifiable crustal anisotropic contrast is clearly associated with the isotropic Moho, suggesting a contrast between the lower crust and the uppermost mantle, similar to what we observe beneath all three of the Grenville stations.

What are the implications of our findings about anisotropic layering at crustal depths for our understanding of past tectonic deformation? First, our inference of a contrast in anisotropic properties across the Moho at four of our stations (ACISO, BINY, ERPA, and TZTN) suggests significant, “frozen-in” anisotropy in the relatively shallow portions of the lithosphere (lower crust and/or uppermost mantle) due to deformation associated with past tectonic

events. The character of the transverse RFs in the time range associated with the Moho does not strictly require anisotropy in the lowermost crust beneath these four stations, but it does imply anisotropy in the deepest crust, the shallowest mantle, or both. In either case, our observations suggest past deformation at depths near the Moho, with enough strain to develop coherent CPO of anisotropic minerals. Second, our observations argue strongly for multiple anisotropic layers within the crust, at middle to lower crustal depths, beneath two of our stations (MCWV and SSPA), both located within the Appalachian Mountains. We interpret this finding as suggesting that (1) the deep crust has undergone significant deformation in the past and has developed anisotropy via the CPO of crustal minerals, most likely associated with Appalachian orogenesis, and (2) the mineralogy, rheology, and/or deformation geometry varied as a function of depth within the crustal column, resulting in multiple layers of crust with contrasting anisotropic geometries. Our inference of layered crustal anisotropy in the ancient Appalachian orogeny is similar to inferences from modern orogens such as Tibet (Liu et al., 2015) and Taiwan (Huang et al., 2015), and provides additional support for the hypothesis that crustal deformation in orogenic systems is complex, varies with depth, and extends to the deep crust.

Regarding the lithospheric mantle, we examine the character of transverse component RFs at time ranges associated with anisotropic and/or dipping contrasts within the lithospheric mantle, shown in Figure 8. Of particular interest are the possible relationships between contrasts in anisotropy and the MLDs inferred from the single-station radial RF stacks shown in Figure 3. The term mid-lithospheric discontinuity, coined by Abt et al. (2010), refers to a sharp decrease in seismic velocity at a depth internal to the continental mantle lithosphere. MLDs have been documented in a number of continental regions (e.g., Abt et al., 2010; Ford et al., 2010; Foster et al., 2014; Hopper et al., 2014; Hopper and Fischer, 2015), although their origin remains debated (e.g., Selway et al., 2015; Karato et al., 2015; Rader et al., 2015). Several workers have suggested a link between anisotropic layering in the continental lithosphere and the observation of MLDs (e.g., Yuan and Romanowicz, 2010; Sodoudi et al., 2013; Wirth and Long, 2014). In particular, our previous work using data from the Granite-Rhyolite Province of North America (Wirth and Long, 2014) found evidence for a clear contrast in anisotropy in the same depth range ( $\sim 90$  km) as the MLD, although our observations also required a decrease in isotropic seismic velocity with depth and could not be

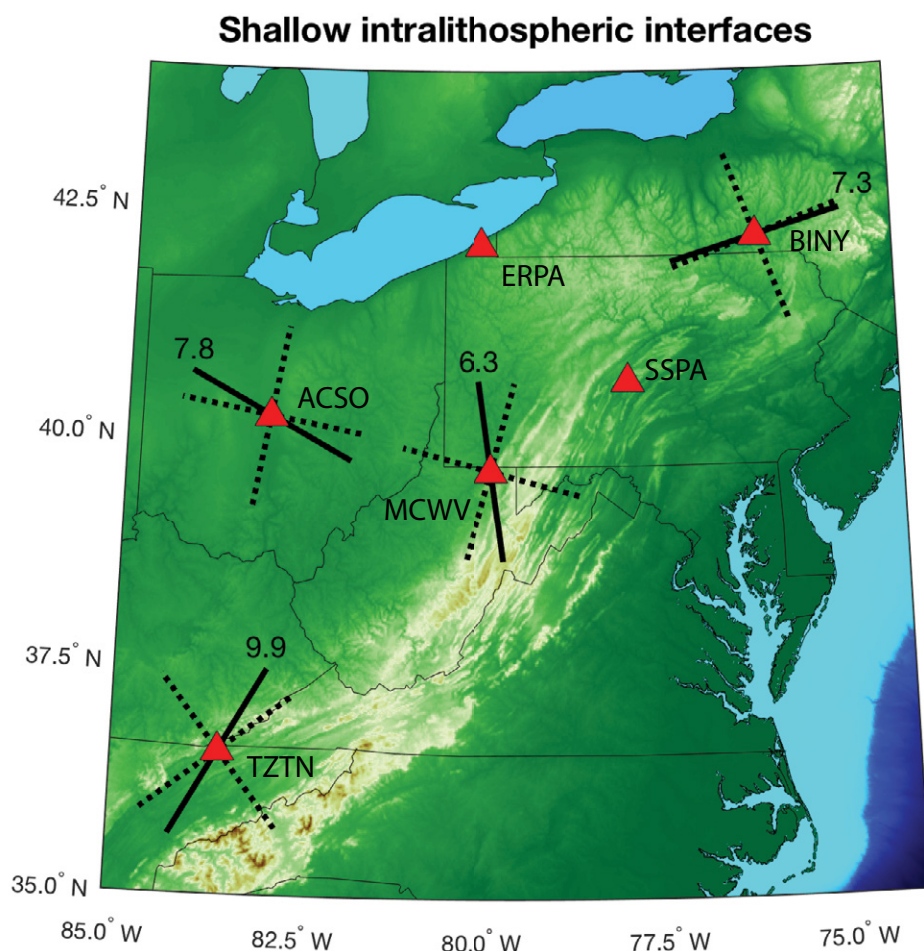


**Figure 10.** Summary map of the properties of shallow intralithospheric interfaces as derived from the harmonic expansion. Here we plot anisotropic contrasts within the shallow mantle lithosphere that do not correspond to isotropic velocity drops (those interfaces are shown in Fig. 11). Stations ERPA and SSPA do not overlie any such interfaces. As in Figure 9, solid lines show the azimuthal phase information for the  $k = 1$  terms in the harmonic expansion, while dotted lines show the azimuthal phase information for the  $k = 2$  terms in the harmonic expansion. Each of the  $k = 1$  orientations is marked with the arrival time of the Ps converted phase (relative to direct P wave arrival).

explained solely by anisotropic layering within the lithosphere.

Figure 8 demonstrates the presence of complex dipping and/or anisotropic layering within the lithospheric mantle beneath the eastern United States, with 2–3 clear interfaces that correspond clearly to transverse RF polarity changes with backazimuth, arriving  $\sim 7$ – $12$  s after the P arrival, identified at each station. This finding is similar to our previous work using data from the Superior and Wyoming cratons in North America (Ford et al., 2016), where we typically identified multiple layers of anisotropy within the mantle lithosphere. Comparing the rose diagrams in Figure 8 to the single-station radial component RF stacks in Figure 3, we can evaluate whether there is a correspondence (in converted wave arrival timing and thus in interface depth) between isotropic MLDs (corresponding to red or negative

pulses in Fig. 3) and contrasts in anisotropy and/or dipping interfaces (as inferred from the harmonic decomposition and illustrated with rose diagrams in Fig. 8). Beneath stations ACISO, ERPA, MCWV, and SSPA, we are able to identify interfaces that apparently exhibit both an isotropic drop in velocity with depth as well as an anisotropic or dipping character. For example, beneath ACISO there is a clear discontinuity that produces a negative pulse on the stacked radial RFs at 9.5 s; the corresponding rose diagram in Figure 8 exhibits clear backazimuthal variations that include an anisotropic component. Similarly, beneath SSPA there are two clear negative pulses on the stacked radial RFs (at  $t = 6.9$  s and 10.3 s) that also require a contrast in anisotropy, likely with a dipping component (nonzero amplitudes in the  $k = 1$  and  $k = 2$  stacks in Fig. 6). However, again similar to the findings of Ford et al.

(2016), we do not observe a simple, one to one correspondence between the isotropic MLD arrivals and the anisotropic interfaces. Rather, we observe complex layering within the lithosphere with both anisotropic and isotropic interfaces, and only sporadic correlations between isotropic and anisotropic structure.

Constraints on the geometry of the RF polarity changes due to anisotropic and/or dipping interfaces beneath our stations are visualized in map view in Figures 9–11, which show the phase orientation information for the  $k = 1$  and  $k = 2$  terms in the harmonic expansion for a series of interfaces at different depths. These directions are derived from measurements of the relative amplitudes of the sine and cosine terms, and denote the possible orientations that may correspond to the dip direction (for a dipping interface) or the plunge direction (for a plunging symmetry axis) for the  $k = 1$  terms, and contain information about contrasts across interfaces in symmetry axis orientation (for azimuthal anisotropy) for the  $k = 2$  terms. We caution that these orientations do not uniquely constrain the geometry of anisotropy or of dipping interfaces; in the absence of detailed forward modeling, assumptions must be made about the properties of individual layers in order to estimate the anisotropic geometry. Nevertheless, the phase data contain some information about possible dip orientations and about the geometrical relationships between azimuthally anisotropic symmetry directions across interfaces (e.g., Shiomi and Park, 2008; Schulte-Pelkum and Mahan, 2014a, 2014b; Olugboji and Park, 2016), and regional variations in the possible orientations can be easily evaluated in map view.

Figure 9 shows the phase information for interfaces within the crust and across the Moho for those stations where the Moho interface includes a dipping and/or anisotropic component. This map reveals significant lateral variability in the character of crustal interfaces across the study region, and little in the way of straightforward relationships between the phase orientations and geologic and tectonic indicators. In Figure 10, we show phase orientations for interfaces internal to the lithosphere that do not correspond to strong isotropic contrasts in velocity; rather, these are shallow intralithospheric contrasts in anisotropy, typically with a dipping axis of symmetry. As with the crustal interfaces in Figure 9, we observe a great deal of regional variability. In Figure 11, we show orientations for interfaces in the mid-lithosphere that exhibit both an isotropic drop in velocity with depth, thus corresponding to isotropic MLDs, as well as a dipping and/or anisotropic character. There is some consistency between the  $k = 1$  phase orientations at stations ERPA, MCWV, and SSPA,

## Co-existing with isotropic MLDs

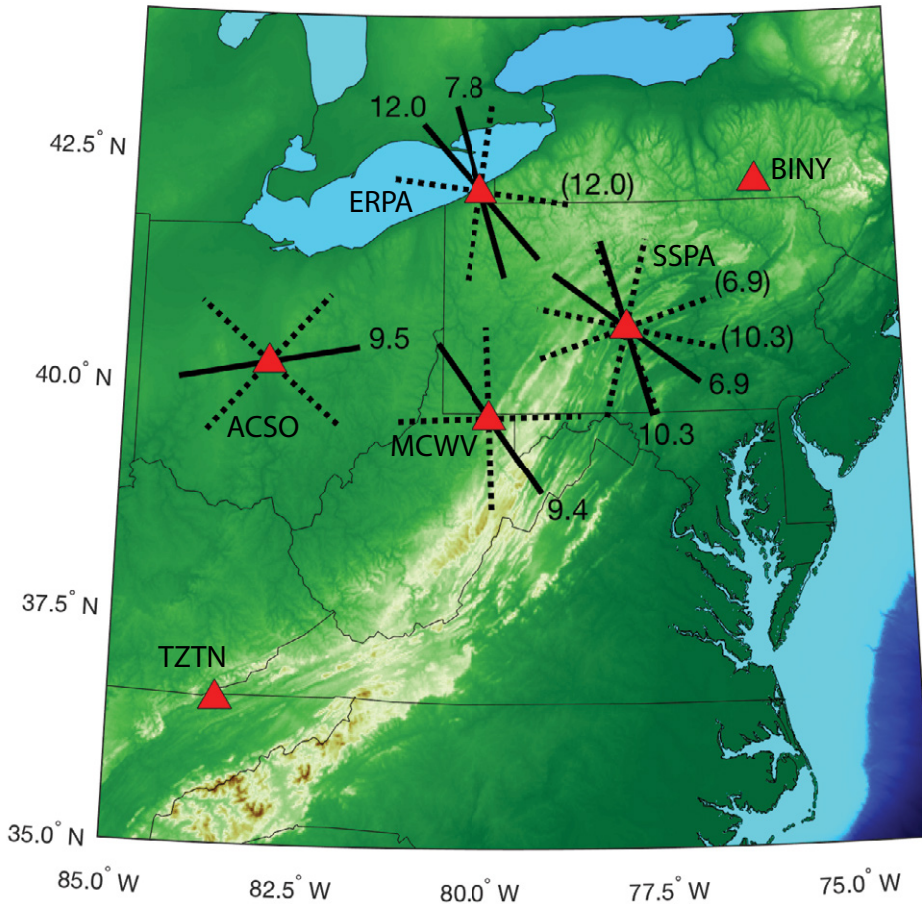


**Figure 11.** Summary map of the properties of mid-lithospheric interfaces as derived from the harmonic decomposition. Here we only show those interfaces that correspond to both an isotropic velocity decrease (i.e., that have a strong negative  $k = 0$  term in the harmonic expansion) and to a contrast in anisotropy and/or a dip, as inferred from the  $k = 1$  and  $k = 2$  terms. Plotting conventions are as in Figure 10. Note that stations BINY and TZTN do not exhibit such interfaces, while stations ERPA and SSPA both exhibit multiple interfaces. For ERPA, one of those (arrival time at 7.8 s) is described well with only  $k = 1$  terms, so no  $k = 2$  terms are shown. At SSPA and ERPA, we label the Ps arrival time for  $k = 2$  components in parentheses to distinguish the multiple interfaces.

two of which (ERPA and SSPA) exhibit multiple anisotropic MLD interfaces. All of these have  $k = 1$  orientations directed approximately northwest-southeast, with more variability in the  $k = 2$  phase information.

A direct comparison between our results and those in Wirth and Long (2014) is instructive, particularly for stations ACISO and ERPA, which are located within the Granite-Rhyolite Province (ACISO) or in the adjacent and related Elzevir block (ERPA). Figure 8 shows rose diagrams for arrivals in the time range between ~7.8 and 10.5 s (corresponding to depths between ~80–105 km) at Granite-Rhyolite stations; at each of these stations, evidence for layered anisotropy within the mantle lithosphere was identified (Wirth and Long, 2014) with conversions from one or more anisotropic interfaces

arriving in the same time range as conversions from the isotropic MLD. Furthermore, at three of the Granite-Rhyolite stations (BWI, BLO, and CCM), the transverse component RFs associated with the main MLD interface exhibited similar behavior, with four clear changes in polarity across the full backazimuthal range. A forward model of the data at station WCI (Wirth and Long, 2014) invokes three lithospheric layers of anisotropy; across the likely main MLD interface, the upper model layer has an approximately north-south anisotropic fast direction and the lower layer is nearly east-west. This model geometry predicts polarity changes similar to those observed at WCI (Fig. 8, lower left), with negative transverse component arrivals in the northeast and southwest quadrants and positive arrivals in the northwest and southeast

quadrants. A comparison of this specific geometric pattern with the transverse RF behavior at stations ERPA and ACISO in similar time ranges (Fig. 8, upper right) demonstrates that the backazimuthal patterns are distinctly different beneath the Grenville stations in our study. The fact that station ACISO in particular, which is also located within the Granite-Rhyolite Province (similar to nearby stations BLO and WCI from Wirth and Long, 2014) but to the east of the Grenville Front, does not exhibit a similar geometric pattern implies that the lithosphere beneath ACISO was modified via subsequent deformation. We suggest that this lithosphere was deformed during Grenville orogenesis, thus modifying the preexisting lithospheric structure that is still present elsewhere in the mantle of the Granite-Rhyolite Province.

How do our observations compare to other previous inferences on the anisotropy of the crust and mantle lithosphere beneath eastern North America? In general terms, our results are consistent with previous work that has suggested a significant contribution to seismic observations from anisotropy in the mantle lithosphere, based on surface waves (e.g., Deschamps et al., 2008), SKS splitting patterns (e.g., Long et al., 2016), or on combinations of different types of data (e.g., Yuan and Romanowicz, 2010; Yuan and Levin, 2014). Recent work on Pn velocities and anisotropy beneath the continental United States (Buehler and Shearer, 2017) also suggests significant anisotropy in the uppermost mantle beneath our study region; Buehler and Shearer (2017) further propose that there must be multiple layers of anisotropy within the upper mantle, potentially consistent with our observations of anisotropic layering within the mantle lithosphere. Our finding of significant anisotropic layering with the middle to lower crust beneath at least some of our stations is also generally consistent with results of Schulte-Pelkum and Mahan (2014a), who suggested crustal anisotropy (often with a plunging symmetry axis) beneath a number of USArray Transportable Array (TA) stations in the eastern United States, particularly in the Appalachians (see their Fig. 8). It is interesting that our finding that the layered anisotropic structure of the mantle lithosphere differs across the Grenville deformation front contrasts with the view provided by shear wave splitting observations, which reflect an integrated signal from the entire upper mantle. For example, Sénéchal et al. (1996) observed similar SKS splitting on either side of the Grenville Front in Canada, while in Long et al. (2016) it was noted that there is no obvious correlation between SKS splitting patterns measured at TA stations and the geometry of the Grenville Front in the eastern and central United States.

A major limitation of the anisotropic RF technique is that while we can confidently infer the presence (and roughly estimate the depths) of anisotropic interfaces within the lithosphere, as well as some orientation information from the  $k = 1$  and  $k = 2$  phase values from the harmonic stacking, it is difficult to infer the geometry of anisotropy within each layer without detailed forward modeling. Such forward modeling is computationally intensive and nonunique, with a large number of unknown parameters, so while it can identify plausible models, it often cannot uniquely determine the anisotropy geometry in every layer. These difficulties can be ameliorated by the use of model space search approaches (e.g., Porter et al., 2011; Wirth et al., 2017) or Bayesian inversion schemes (e.g., Bodin et al., 2016), but there are still strong tradeoffs among parameters. In lieu of detailed forward modeling, the harmonic decomposition modeling applied here (or approaches similar to it; e.g., Schulte-Pelkum and Mahan, 2014a) can identify interfaces and provide some primary information about their geometry by examining the relative amplitudes and phases of the  $k = 0, 1, 2$  terms, and provides a natural way of comparing structure among different stations. Furthermore, the RF observations and the harmonic decomposition models presented in this paper can serve as a starting point for future detailed forward modeling, ideally in combination with other data that constrain seismic anisotropy (such as SKS splitting observations, surface wave dispersion, and/or Pn traveltimes). One example of this type of modeling was discussed by Yuan and Levin (2014), who combined different types of anisotropy observations, including backazimuthal RF gathers, into a forward model of multilayered anisotropy beneath three stations in the eastern United States (including SSPA, one of the stations examined in this study).

Despite the limitations of the RF technique, the observations presented in this paper allow us to draw some straightforward inferences about lithospheric deformation beneath the eastern United States and its likely causes. Our identification of extensive anisotropy in the deep crust and mantle lithosphere beneath each of the stations examined in this study implies extensive lithospheric deformation, with enough strain to generate significant CPO. While it is not possible to conclusively identify the deformation events and their timing and geometry, we suggest that the last major orogenic cycle to affect each region is the most plausible tectonic event to have caused widespread lithospheric deformation (e.g., Meissner et al., 2002). Therefore, we propose that the anisotropic structure of the mantle lithosphere beneath ACSO, ERPA, and BINY was shaped by deformation associated

with the Grenville orogenic cycle, while Appalachian orogenesis caused lithospheric deformation beneath SSPA, MCWV, and TZTN. Our observations strongly suggest anisotropic layering within the crust beneath two of the three Appalachian stations examined, with an anisotropic geometry that varies with depth. This finding is similar to the documentation of crustal anisotropy in modern mountain belts (e.g., Liu et al., 2015; Huang et al., 2015), and suggests complex crustal deformation accompanying orogenesis. Our main finding of extensive but layered deformation within the lithospheric mantle (at depths to  $\sim 100$  km) presents an interesting challenge to the classic idea of vertically coherent deformation (Silver, 1996). Although our observations suggest that the geometry of anisotropy (and thus deformation) changes with depth, they also suggest significant deformation throughout much of the lithosphere associated with orogenesis. This is consistent with the suggestion by Silver (1996) that the lithosphere participates in deformation, leading to seismic anisotropy, but the finding of changes in anisotropic geometry with depth suggests that the geometry of deformation and/or of olivine fabric development is not coherent over the entire lithospheric mantle.

Our identification of lithospheric anisotropy beneath eastern North America is consistent with observations in other continental regions, including those that have undergone (or are currently undergoing) orogenesis (e.g., Meissner et al., 2002; Wüstefeld et al., 2010). Our main conclusions are also consistent with the many previous suggestions that SKS splitting in and around the Appalachians, which is typically parallel to the mountain belt (at least in the central and southern portions), reflects a significant contribution from lithospheric anisotropy (e.g., Barruol et al., 1997; Wagner et al., 2012; Long et al., 2016). We also note that our inference of multiple layers of anisotropy within the mantle lithosphere is generally consistent with the surface wave model of Deschamps et al. (2008) for a region just to the south and west of our study area. Although there is no substantial geographic overlap between our study region and that of Deschamps et al. (2008), we discussed the similarities and differences between the model of Deschamps et al. (2008) and models derived from RFs in our previous work (Wirth and Long, 2014).

## SUMMARY

We examined data from six long-running broadband seismic stations located within regions of the eastern United States that were affected by the Grenville and Appalachian

orogenic cycles. We computed radial and transverse RFs and applied a harmonic stacking method that allows us to identify interfaces within the crust and lithospheric mantle that have a dipping and/or anisotropic character, in addition to interfaces that can be explained in terms of an isotropic velocity contrast. We find evidence for layered anisotropy, often with a likely dipping axis of symmetry, beneath all stations examined in this study. There is often a clear anisotropic contrast associated with the Moho interface, requiring anisotropy in the lowermost crust, the uppermost mantle, or both. Similar to recent findings within Archean regions of North America, we find evidence for complex anisotropic layering with the mantle lithosphere. At two of the stations in the Appalachian Mountains, we observe clear evidence for anisotropic contrasts within the crust, suggesting middle to lower crustal deformation associated with Appalachian orogenesis. A detailed comparison between our observations and previous anisotropic RF analysis at stations located in the Granite-Rhyolite Province but to the west of the Grenville Front suggests a different geometry of anisotropy in the mantle lithosphere. This, in turn, suggests that the lithospheric mantle just to the east of the Grenville Front was deformed during the Grenville orogenic cycle. Our observations can provide a starting point for the future testing of detailed deformation scenarios associated with past tectonic events, ideally in combination with other types of data that constrain seismic anisotropy.

## ACKNOWLEDGMENTS

Seismic waveform data from the U.S. National Seismic Network and the Global Seismographic Network were accessed via the Data Management Center of the Incorporated Research Institutions for Seismology (IRIS). Some figures were prepared using Generic Mapping Tools (Wessel and Smith, 1999). This work was carried out in part through the IRIS Summer Internship Program and was funded by the EarthScope program of the National Science Foundation via grant EAR-1358325. We thank Juan Aragon, Maggie Benoit, Vadim Levin, and Jeffrey Park for helpful discussions and two anonymous reviewers for thoughtful and constructive comments that improved the paper.

## REFERENCES CITED

- Abt, D.L., Fischer, K.M., French, S.W., Ford, H.A., Yuan, H., and Romanowicz, B., 2010, North American lithospheric discontinuity structure imaged by *Ps* and *Sp* receiver functions: *Journal of Geophysical Research*, v. 115, B09301, doi:10.1029/2009JB006914.
- Allen, J.S., Thomas, W.A., and Lavoie, D., 2010, The Laurentian margin of northeastern North America, in Tollo, R.P., et al., eds., *From Rodinia to Pangea: The Lithotectonic Record of the Appalachian Region*: Geological Society of America Memoir 206, p. 71–90, doi:10.1130/2010.1206(04).
- Barruol, G., Silver, P.G., and Vauchez, A., 1997, Seismic anisotropy in the eastern United States: Deep structure of a complex continental plate: *Journal of Geophysical Research*, v. 102, p. 8329–8348, doi:10.1029/96JB03800.
- Bartholomew, M.J., and Hatcher, R.D., Jr., 2010, The Grenville orogenic cycle of southern Laurentia: Unraveling sutures, rifts, and shear zones as potential piercing points for Amazonia: *Journal of South American Earth Sciences*, v. 29, p. 4–20, doi:10.1016/j.jsames.2009.08.007.

- Bartholomew, M.J., and Whitaker, A.E., 2010, The Alleghanian deformational sequence at the foreland junction of the Central and Southern Appalachians, *in* Tollo, R.P., et al., eds., From Rodinia to Pangea: The Lithotectonic Record of the Appalachian Region: Geological Society of America Memoir 206, p. 431–454, doi:10.1130/2010.1206(19)
- Benoit, M.H., Ebinger, C., and Crampton, M., 2014, Orogenic bending around a rigid Proterozoic magmatic rift beneath the Central Appalachian Mountains: Earth and Planetary Science Letters, v. 402, p. 197–208, doi:10.1016/j.epsl.2014.03.064.
- Bianchi, I., Park, J., Piana Agostinetti, N., and Levin, V., 2010, Mapping seismic anisotropy using harmonic decomposition of receiver functions: An application to Northern Apennines, Italy: Journal of Geophysical Research, v. 115, B12317, doi:10.1029/2009JB007061.
- Bodin, T., Leiva, J., Romanowicz, B., Maupin, V., and Yuan, H., 2016, Imaging anisotropic layering with Bayesian inversion of multiple data types: Geophysical Journal International, v. 206, p. 605–629, doi:10.1093/gji/ggw124.
- Bostock, M.G., 1998, Mantle stratigraphy and evolution of the Slave province: Journal of Geophysical Research, v. 103, p. 21,183–21,200, doi:10.1029/98JB01069.
- Buehler, J.S., and Shearer, P.M., 2017, Uppermost mantle seismic velocity structure beneath USArray: Journal of Geophysical Research, v. 122, p. 436–448, doi:10.1002/2016JB013265.
- Burton, W.C., and Southworth, S., 2010, A model for Iapetan rifting of Laurentia based on Neoproterozoic dikes and related rocks, *in* Tollo, R.P., et al., eds., From Rodinia to Pangea: The Lithotectonic Record of the Appalachian Region: Geological Society of America Memoir 206, p. 455–476, doi:10.1130/2010.1206(20).
- Cawood, P.A., and Buchan, C., 2007, Linking accretionary orogenesis with supercontinent assembly: Earth-Science Reviews, v. 82, p. 217–256, doi:10.1016/j.earscirev.2007.03.003.
- Culotta, R.C., Pratt, T., and Oliver, J., 1990, A tale of two sutures: COCORP's deep seismic surveys of the Grenville province in the eastern U.S. midcontinent: Geology, v. 18, p. 646–649, doi:10.1130/0091-7613(1990)018<0646:ATOTSC>2.3.CO;2.
- Deschamps, F., Lebedev, S., Meier, T., and Trampert, J., 2008, Stratified seismic anisotropy reveals past and present deformation beneath the east-central United States: Earth and Planetary Science Letters, v. 274, p. 489–498, doi:10.1016/j.epsl.2008.07.058.
- Ford, H.A., Fischer, K.M., Abt, D.L., Rychert, C.A., and Elkins-Tanton, L.T., 2010, The lithosphere-asthenosphere boundary and cratonic lithospheric layering beneath Australia from Sp wave imaging: Earth and Planetary Science Letters, v. 300, p. 299–310, doi:10.1016/j.epsl.2010.10.007.
- Ford, H.A., Long, M.D., and Wirth, E.A., 2016, Mid-lithospheric discontinuities and complex anisotropic layering in the mantle lithosphere beneath the Wyoming and Superior Provinces: Journal of Geophysical Research, v. 121, p. 6675–6697, doi:10.1029/2016JB012978.
- Foster, K., Dueker, K., Schmandt, B., and Yuan, H., 2014, A sharp cratonic lithosphere-asthenosphere boundary beneath the American Midwest and its relation to mantle flow: Earth and Planetary Science Letters, v. 402, p. 82–89, doi:10.1016/j.epsl.2013.11.018.
- Fouch, M.J., and Rondenay, S., 2006, Seismic anisotropy beneath stable continental interiors: Physics of the Earth and Planetary Interiors, v. 158, p. 292–320, doi:10.1016/j.pepi.2006.03.024.
- Frederiksen, A.W., and Bostock, M.G., 2000, Modelling teleseismic waves in dipping anisotropic structures: Geophysical Journal International, v. 141, p. 401–412, doi:10.1046/j.1365-246x.2000.00090.x.
- Frizon de Lamotte, D., Fourdan, B., Leleu, S., Leparmentier, F., and de Clarens, P., 2015, Style of rifting and the stages of Pangea breakup: Tectonics, v. 34, p. 1009–1029, doi:10.1002/2014TC003760.
- Geiser, P., and Engelder, T., 1983, The distribution of layer parallel shortening fabrics in the Appalachian foreland of New York and Pennsylvania: Evidence for two non-coaxial phases of the Alleghanian orogeny, *in* Hatcher, R.D., Jr., et al., eds., Contributions to the Tectonics and Geophysics of Mountain Chains: Geological Society of America Memoir 158, p. 161–176, doi:10.1130/MEM158-p161.
- Hatcher, R.D., Jr., 2010, The Appalachian orogeny: A brief summary, *in* Tollo, R.P., et al., eds., From Rodinia to Pangea: The Lithotectonic Record of the Appalachian Region: Geological Society of America Memoir 206, p. 1–19, doi:10.1130/2010.1206(01).
- Hibbard, J.P., van Staal, C.R., and Rankin, D.W., 2010, Comparative analysis of the geological evolution of the northern and southern Appalachian orogeny: Late Ordovician–Permian, *in* Tollo, R.P., et al., eds., From Rodinia to Pangea: The Lithotectonic Record of the Appalachian Region: Geological Society of America Memoir 206, p. 51–69, doi:10.1130/2010.1206(03).
- Hopper, E., and Fischer, K.M., 2015, The meaning of midlithospheric discontinuities: A case study in the northern U.S. craton: Geochemistry, Geophysics, Geosystems, v. 16, p. 4057–4083, doi:10.1002/2015GC006030.
- Hopper, E., Ford, H.A., Fischer, K.M., Lekic, V., and Fouch, M.J., 2014, The lithosphere-asthenosphere boundary and the tectonic and magmatic history of the northwestern United States: Earth and Planetary Science Letters, v. 402, p. 69–81, doi:10.1016/j.epsl.2013.12.016.
- Huang, T.-Y., Gung, Y., Kuo, B.-Y., Chiao, L.-Y., and Chen, Y.-N., 2015, Layered deformation in the Taiwan orogen: Science, v. 349, p. 720–723, doi:10.1126/science.aab1879.
- Karabinos, P., Samson, S.D., Hepburn, J.C., and Stol, H.M., 1998, Taconian orogeny in the New England Appalachians: Collision between Laurentia and the Shelburne Falls arc: Geology, v. 26, p. 215–218, doi:10.1130/0091-7613(1998)026<0215:TOITNE>2.3.CO;2.
- Karato, S., Jung, H., Katayama, I., and Skemer, P., 2008, Geodynamic significance of seismic anisotropy of the upper mantle: New insights from laboratory studies: Annual Review of Earth and Planetary Sciences, v. 36, p. 59–95, doi:10.1146/annurev.earth.36.031207.124120.
- Karato, S., Oluogboji, T., and Park, J., 2015, Mechanisms and geologic significance of the mid-lithosphere discontinuity in the continents: Nature Geoscience, v. 8, p. 509–514, doi:10.1038/ngeo2462.
- Kennett, B.L.N., Engdahl, E.R., and Buland, R., 1995, Constraints on seismic velocities in the Earth from travel times: Geophysical Journal International, v. 122, p. 108–124, doi:10.1111/j.1365-246X.1995.tb03540.x.
- Ko, B., and Jung, H., 2015, Crystal preferred orientation of an amphibole experimentally deformed by simple shear: Nature Communications, v. 6, 6586, doi:10.1038/ncomms7586.
- Langston, C.A., 1979, Structure under Mount Rainier, Washington, inferred from teleseismic body waves: Journal of Geophysical Research, v. 84, p. 4749–4762, doi:10.1029/JB084iB09p04749.
- Levin, V., and Park, J., 1997, *P-SH* conversions in a flat-layered medium with anisotropy of arbitrary orientation: Geophysical Journal International, v. 131, p. 253–266, doi:10.1111/j.1365-246X.1997.tb01220.x.
- Levin, V., and Park, J., 1998, *P-SH* conversions in layered media with hexagonally symmetric anisotropy: A cookbook: Pure and Applied Geophysics, v. 151, p. 669–697, doi:10.1007/s000240050136.
- Levin, V., Menke, W., and Park, J., 1999, Shear wave splitting in the Appalachians and the Urals: A case for multilayered anisotropy: Journal of Geophysical Research, v. 104, p. 17,975–17,993, doi:10.1029/1999JB900168.
- Levin, V., Van Tongeren, J.A., and Servati, A., 2016, How sharp is the sharp Archean Moho? Example from eastern Superior Province: Geophysical Research Letters, v. 43, p. 1928–1933, doi:10.1002/2016GL067729.
- Li, Z.X., et al., 2008, Assembly, configuration, and break-up history of Rodinia: A synthesis: Precambrian Research, v. 160, p. 179–210, doi:10.1016/j.precamres.2007.04.021.
- Liu, Z., and Park, J., 2017, Seismic receiver function interpretation: Ps splitting or anisotropic underplating?: Geophysical Journal International, v. 208, p. 1332–1341, doi:10.1093/gji/ggw455.
- Liu, Z., Park, J., and Rye, D.M., 2015, Crustal anisotropy in northeastern Tibetan Plateau inferred from receiver functions: Rock textures caused by metamorphic fluids and lower crust flow?: Tectonophysics, v. 661, p. 66–80, doi:10.1016/j.tecto.2015.08.006.
- Long, M.D., and Silver, P.G., 2009, Shear wave splitting and mantle anisotropy: Measurements, interpretations, and new directions: Surveys in Geophysics, v. 30, p. 407–461, doi:10.1007/s10712-009-9075-1.
- Long, M.D., Benoit, M.H., Chapman, M.C., and King, S.D., 2010, Upper mantle seismic anisotropy and transition zone thickness beneath southeastern North America and implications for mantle dynamics: Geochemistry, Geophysics, Geosystems, v. 11, Q10012, doi:10.1029/2010GC003247.
- Long, M.D., Jackson, K.G., and McNamara, J.F., 2016, SKS splitting beneath Transportable Array stations in eastern North America and the signature of past lithospheric deformation: Geochemistry, Geophysics, Geosystems, v. 17, p. 2–15, doi:10.1002/2015GC006088.
- McCormack, K., Wirth, E.A., and Long, M.D., 2013, B-type olivine fabric and mantle wedge serpentinization beneath the Ryukyu arc: Geophysical Research Letters, v. 40, p. 1697–1702, doi:10.1002/grl.50369.
- McHone, J.G., 1996, Broad-terrace Jurassic flood basalts across northeastern North America: Geology, v. 24, p. 319–322, doi:10.1130/0091-7613(1996)024<0319:BTJFBA>2.3.CO;2.
- McHone, J.G., 2000, Non-plume magmatism and tectonics during the opening of the central Atlantic Ocean: Tectonophysics, v. 316, p. 287–296, doi:10.1016/S0040-1951(99)00260-7.
- McLelland, J., Daly, J.S., and McLelland, J.M., 1996, The Grenville orogenic cycle (ca. 1350–1000 Ma): An Adirondack perspective: Tectonophysics, v. 265, p. 1–28, doi:10.1016/S0040-1951(96)00144-8.
- McLelland, J.M., Selleck, M.W., and Bickford, M.E., 2010, Review of the Proterozoic evolution of the Grenville Province, its Adirondack outlier, and the Mesoproterozoic inliers of the Appalachians, *in* Tollo, R.P., et al., eds., From Rodinia to Pangea: The Lithotectonic Record of the Appalachian Region: Geological Society of America Memoir 206, p. 21–49, doi:10.1130/2010.1206(02).
- Meissner, R., Mooney, W.D., and Artemieva, I., 2002, Seismic anisotropy and mantle creep in young orogens: Geophysical Journal International, v. 149, p. 1–14, doi:10.1046/j.1365-246X.2002.01628.x.
- Moore, J.M., and Thompson, P., 1980, The Flinton Group: A late Precambrian metasedimentary sequence in the Grenville Province of eastern Ontario: Canadian Journal of Earth Sciences, v. 17, p. 1685–1707, doi:10.1139/e80-178.
- Oluogboji, T.M., and Park, J., 2016, Crustal anisotropy beneath Pacific Ocean islands from harmonic decomposition of receiver functions: Geochemistry, Geophysics, Geosystems, v. 17, p. 810–832, doi:10.1002/2015GC006166.
- Park, J., and Levin, V., 2000, Receiver functions from multiple-taper spectral correlation estimates: Bulletin of the Seismological Society of America, v. 90, p. 1507–1520, doi:10.1785/0119990122.
- Park, J., and Levin, V., 2016, Anisotropic shear zones revealed by back-azimuthal harmonics of teleseismic receiver functions: Geophysical Journal International, v. 207, p. 1216–1243, doi:10.1093/gji/ggw323.
- Porter, R., Zandt, G., and McQuarrie, N., 2011, Pervasive lower-crustal seismic anisotropy in southern California: Evidence for underplated schists and active tectonics: Lithosphere, v. 3, p. 201–220, doi:10.1130/L126.1.
- Rader, E., Emry, E., Schmerr, N., Frost, D., Cheng, C., Menard, J., Yu, C.-O., and Geist, D., 2015, Characterization and petrological constraints of the midlithospheric discontinuity: Geochemistry, Geophysics, Geosystems, v. 16, p. 3484–3504, doi:10.1002/2015GC005943.
- Rivers, T., 1997, Lithotectonic elements of the Grenville Province: Review and tectonic implications: Precambrian Research, v. 86, p. 117–154, doi:10.1016/S0301-9268(97)00308-7.
- Sacks, P.E., and Secor, D.T., Jr., 1990, Kinematics of late Paleozoic continental collision between Laurentia and Gondwana: Science, v. 250, p. 1702–1705, doi:10.1126/science.250.4988.1702.
- Schlichte, R.W., Withjack, M.O., and Olson, P.E., 2003, Relative timing of CAMP, rifting, continental breakup, and basin inversion: Tectonic significance, *in* Hames, W.E., et al., eds., The Central Atlantic Magmatic Province: Insights from fragments of Pangea: American Geophysical Union Geophysical Monograph 136, p. 33–59, doi:10.1029/136GM03.
- Schulte-Pelkum, V., and Mahan, K.H., 2014a, A method for mapping crustal deformation and anisotropy with receiver functions and first results from USArray: Earth and Planetary Science Letters, v. 402, p. 221–233, doi:10.1016/j.epsl.2014.01.050.
- Schulte-Pelkum, V., and Mahan, K.H., 2014b, Imaging faults and shear zones using receiver functions: Pure and

- Applied Geophysics, v. 171, p. 2967–2991, doi:10.1007/s00024-014-0853-4.
- Selway, K., Ford, H., and Kelemen, P., 2015, The seismic mid-lithosphere discontinuity: Earth and Planetary Science Letters, v. 414, p. 45–57, doi:10.1016/j.epsl.2014.12.029.
- Sénéchal, G., Rondenay, S., Mareschal, M., Guilbert, J., and Poupinet, G., 1996, Seismic and electrical anisotropies in the lithosphere across the Grenville Front, Canada: Geophysical Research Letters, v. 23, p. 2255–2258, doi:10.1029/96GL01410.
- Shiomi, K., and Park, J., 2008, Structural features of the subducting slab beneath the Kii Peninsula, central Japan: Seismic evidence of slab segmentation, dehydration, and anisotropy: Journal of Geophysical Research, v. 113, B10318, doi:10.1029/2007JB005535.
- Silver, P.G., 1996, Seismic anisotropy beneath the continents: Probing the depths of geology: Annual Review of Earth and Planetary Sciences, v. 24, p. 385–432, doi:10.1146/annurev.earth.24.1.385.
- Sodoudi, F., Yuan, X., Kind, R., Lebedev, S., Adam, J.M.C., Kastle, E., and Tilmann, F., 2013, Seismic evidence for stratification in composition and anisotropic fabric within the thick lithosphere of the Kalahari Craton: Geochemistry, Geophysics, Geosystems, v. 14, p. 5393–5412, doi:10.1002/2013GC004955.
- Thomas, W.A., 2004, Tectonic inheritance at a continental margin: GSA Today, v. 16, p. 4–11, doi:10.1130/1052-5173(2006)016<4:TIAACM>2.0.CO;2.
- Tommasi, A., and Vauchez, A., 2015, Heterogeneity and anisotropy in the lithospheric mantle: Tectonophysics, v. 661, p. 11–37, doi:10.1016/j.tecto.2015.07.026.
- Ver Straeten, C.A., 2010, Lessons from the foreland basin: Northern Appalachian basin perspectives on the Acadian orogeny, in Tollo, R.P., et al., eds., From Rodinia to Pangea: The Lithotectonic Record of the Appalachian Region: Geological Society of America Memoir 206, p. 251–282, doi:10.1130/2010.1206(12).
- Wagner, L.S., Long, M.D., Johnston, M.D., and Benoit, M.H., 2012, Lithospheric and asthenospheric contributions to shear-wave splitting observations in the southeastern United States: Earth and Planetary Science Letters, v. 341–344, p. 128–138, doi:10.1016/j.epsl.2012.06.020.
- Ward, D., Mahan, K., and Schulte-Pelkum, V., 2012, Roles of quartz and mica in seismic anisotropy of mylonites: Geophysical Journal International, v. 190, p. 1123–1134, doi:10.1111/j.1365-246X.2012.05528.x.
- Wessel, P., and Smith, W.H.F., 1999, Free software helps map and display data: Eos, v. 72, p. 441–446, doi:10.1029/90EO00319.
- Whitmeyer, S., and Karlstrom, K., 2007, Tectonic model for the Proterozoic growth of North America: Geosphere, v. 3, p. 220–259, doi:10.1130/GES00055.1.
- Wirth, E.A., and Long, M.D., 2012, Multiple layers of seismic anisotropy and a low-velocity region in the mantle wedge beneath Japan: Evidence from teleseismic receiver functions: Geochemistry, Geophysics, Geosystems, v. 13, Q08005, doi:10.1029/2012GC004180.
- Wirth, E.A., and Long, M.D., 2014, A contrast in anisotropy across mid-lithospheric discontinuities beneath the central United States—A relic of craton formation: Geology, v. 42, p. 851–854, doi:10.1130/G35804.1.
- Wirth, E.A., Long, M.D., and Moriarty, J., 2017, A Markov chain Monte Carlo with Gibbs sampling approach to anisotropic receiver function forward modeling: Geophysical Journal International, v. 208, p. 10–23, doi:10.1093/gji/ggw383.
- Wüstefeld, A., Bokelmann, G., and Barruol, G., 2010, Evidence for ancient lithospheric deformation in the East European Craton based on mantle seismic anisotropy and crustal magnetics: Tectonophysics, v. 481, p. 16–28, doi:10.1016/j.tecto.2009.01.010.
- Yang, B.B., Liu, Y., Dahm, H., Liu, K.H., and Gao, S.S., 2017, Seismic azimuthal anisotropy beneath the eastern United States and its geodynamic implications: Geophysical Research Letters, v. 44, p. 2670–2678, doi:10.1002/2016GL071227.
- Yuan, H., and Levin, V., 2014, Stratified seismic anisotropy and the lithosphere-asthenosphere boundary beneath eastern North America: Journal of Geophysical Research, v. 119, p. 3096–3114, doi:10.1002/2013JB010785.
- Yuan, H., and Romanowicz, B., 2010, Lithospheric layering in the North American craton: Nature, v. 466, p. 1063–1068, doi:10.1038/nature09332.

MANUSCRIPT RECEIVED 23 FEBRUARY 2016  
 REVISED MANUSCRIPT RECEIVED 14 JULY 2017  
 MANUSCRIPT ACCEPTED 24 AUGUST 2017

Printed in the USA